SWANSEA UNIVERSITY

ECOLE CENTRALE DE NANTES

UNIVERSITAT POLITECNICA DE CATALUNYA ,CIMNE

Erasmus Mundus Master

Master T H E S I S

to obtain the diploma of

Master of Science

Specialty : Computational Mechanics

Defended by
Haiqin Huang

1D Comparison of Methods to Follow Moving Discontinuities in Dynamics Phase Change

Thesis Advisor: Prof. Nicolas MOËS

prepared at Structure Simulation Team,
GeM Institut, Ecole Centrale de Nantes

defended in Sep, 2014

Jury :

Advisor:	Prof. Nicolas MOËS	-	*Structures et Simulations GeM, ECN*
Invited:	Prof. Laurent Stainier	-	*Structures et Simulations GeM, ECN*
Invited:	Dr. Patrick Rozycki	-	*Structures et Simulations GeM, ECN*

Abstract

Explicit computational methods are investigated in one-dimensional dynamics of solids capable of twinning and phase transitions. In crystal, microstructure changes undergo solid to solid phase changes upon thermal or mechanical loading, can strongly influence physical properties such as strength, toughness, ductility, hardness, corrosion resistance, temperature behavior, wear resistance. These comprise a collection of interfaces between the different phases. A level set as a signed distance function is used to separate the different phases. The evolution of interface is governed by momentum balance, jump conditions and a kinetic relation representing the interface velocity as a function of the driving force. The calculation of the driving force is through the thick level set method, which was originally used in damage in fracture. The stored energy function is nonconvex potential with multiple wells. The interface in sharp interface theory is treated as zero thickness, thus discontinuity occurs in the strain and velocity . These discontinuities will generate nonphysical oscillation when finite element methods are applied. Therefore, the diffuse interface theory is introduced, in which the interfaces are replaced by diffuse layers of non-zero thickness eliminating discontinuities. The classic Lagrangian finite element method and Arbitrary Lagrangian Eulerian (ALE) finite element methods are applied. Besides, a new FiGALE finite element method is proposed, which combines the benefits of Lagrangian mesh and ALE theory. The central difference time integral is chosen as our explicit time integration. Several numerical examples are investigated using two interface theories, sharp interface theory and diffuse interface theory and three numerical methods, Lagrangian ALE and FiGALE finite element methods. Numerical simulations exhibit complex evolution of the interface,the energy evolution, displacement and stress distribution. Results show that FiGALE contains less oscillation in sharp interface theory. In the diffuse interface theory FiGALE results are more close to the referential results while contain small oscillations. Thus, the advantages of FiGALE method is demonstrated by the numerical results. In summary, Lagrangian, ALE and FiGALE finite element methods are demonstrated in one-dimensional solids dynamics problem with phase transitions. The contribution lies in the introduction of thick level set to calculate the driving force and the proposal of FiGALE finite element method.

Keywords: Dynamics; Phase changing; Lagrangian; Arbitrary Lagrangian Eulerian; Finite element methods; Thick level set

Acknowledgments

First of all I would like to express my gratitude to my supervisor, Prof. Nicolas Moës. From the very beginning, his vivid and extraordinary lectures on 'Extended Finite Element Methods' attracted almost all students. It opened me a new window to simulations and methods to deal with discontinuous problems. I am very grateful that he can give me this great opportunity of doing master thesis on discontinuous problems under his guidance. During my thesis, he pays great patience and leads me to do the research step by step. I still remembered his vivid examples when helping me to better understand shock waves. Again, I would like to thank him for his expertise, understanding, and patience, contributing considerably to my graduate experience.

I would like to thank my tutor Dr. Nicolas Chevaugeon for all the help during my master study in Nantes. I am also thankful to Dr. Patrick Rozycki for his kindly help. I must also acknowledge all the other colleagues in Structure Simulation team in Gem Institute. A very special thanks goes out to Dr. Zheng Li for the help during my thesis. It is not easy to use Latex for the beginners. I am very grateful for his meticulous guidance and great patience. Furthermore, I would like to thank my classmates during my master study. I am very glad that we have had the great time of studying together and helping each other, just like comrade-in-arms. Finally, I would like to thank my parents for their love and constant support.

List of Figures

Contents

Chapter 1

Introduction

We are interested in explicit methods for the computation of propagating interfaces in solid materials. The evolution of interfaces is governed by the momentum balances, jump conditions and a kinetic relation representing the interface velocity as a function of the configurational force. A level set as a signed distance function is used to separate the different phases. The evolution of this function is described by a Hamilton-Jacobi equation and its velocity coefficient is determined by the kinetic relation.

In a one-dimensional, sharp interface model of twinning, the stored-energy function is a nonconvex potential with multiple wells. This energy function suffers discontinuities across the interface. These discontinuities will generate nonphysical oscillation when finite element methods are applied to our problem. Thus, the diffuse interface theory is introduced, which contains diffuse layers eliminating the energy jump across the interface.

In solid mechanics, the Lagrangian mesh is widely used. As it involves material velocity and strain discontinuities across the interface, we apply Arbitrary Lagrangian Eulerian (ALE) methods. ALE formulations of the momentum balance are introduced and considering the convectional part, we use Streamline Upwind Petrov Galerkin finite element method to solve the ALE formulations. All these details are demonstrated in Chapter 3.

In Chapter 4, a special treatment of configurational force is introduced as the thick level set, which averages information over the diffuse layer. This thick level set method has been recently used to the fracture damage and has shown advantages. Besides, we propose a new method FiGALE combining the convenience of fixed mesh and the advantages of ALE for moving interfaces.

In Chapter 5, several numerical examples are investigated in Lagrangian mesh, ALE descriptions, and FiGALE method. Results and conclusions are formulated afterwards.

Chapter 2

Bibliography

2.1 Introduction

We are going introduce the methodical models: phase change, sharp interface theory and diffuse interface theory and numerical techniques: finite element methods and explicit time integration.

Many crystals such as crystals undergoing twinning, or shape-memory alloys capable of phase transitions of austenite-martensite type, suffer complex microstructures leading to phase change under certain thermal or mechanical loading. Phase boundaries occurs between different phases or twin interfaces between differently oriented twin lattice variants.

Phase interface evolution is accompanied by energy dissipation and can not been determined only by balance laws of continuum mechanics and jump conditions. A kinetic relation between the interface velocity and the driving or configurational force is introduced. Singularity among the interface is formed in the sharp interface theory with discontinuity surfaces of zero thickness. Standard shock-capturing methods and finite element methods can not be applied to the sharp interface model, thus the diffuse interface theory is applied with level set method.

Arbitrary Lagrangian Eulerian descriptions are introduce to deal with the moving interfaces. It combines both the advantages of Lagrangian and Eulerian descriptions. A survey of literature on finite element methods is conducted to solve the ALE formulations and the Streamline Upwind Petrov Galerkin finite element method shows benefits.

At last, we tour the existing papers to find a good explicit time integration for our phase change dynamics problem.

2.2 Phase Change

Microstructure changes undergo solid to solid phase changes upon thermal or mechanical loading, can strongly influence physical properties such as strength, toughness, ductility, hardness, corrosion resistance, temperature behavior, wear resistance. Their effects to materials can be classified into the shape memory effect (SMA), the transformation-induced plasticity effect (TRIP) or the twinning-induced plasticity effect (TWIP). There are some twinning models in Fig. 2.1

The major deformation modes enabling a solid to change shape are individual atoms being mobile, slip and twinning under the action of an applied stress.

Twinning are found in metals and alloys, other inter-metallic compounds, elemental semiconductors and compounds, other non-metallic compounds like calcite and sodium nitrate and even complex minerals and crystalline polymers. [2] Crystals undergoing twinning reorients its lattice but do not change the the lattice structure like to martensitic transformations. Experiments with single crystals have shown that Face Centered Cubic (FCC) metals do not normally twin until appreciable plastic deformation by slip, while in Body Centered Cubic (BCC) metals twins often form in the elastic region of the stress vs strain curve before macroscopic yielding. [2] In general, delayed twinning has a rather small effect on the actual stress-strain curve, while immediate twinning is characterized by very rapid formation of twinned regions, giving large load drops, and very sensitive to temperature of deformation and to strain rate. [2] For shuffle-free twinning modes, the twin lattice is formed by applying a homogeneous shear deformation to the parent lattice, whereas for twinning modes with shuffling, the homogeneous shear deformation leaves only the atoms of a sub-lattice in their proper twin configuration and the rest atoms undergo a shuffling displacement. [2] In both cases, a regular reordering of the atomic bonding, or interface is observed. The interface propagation determines the dissipation due to the interface movement, while the interface movement can not simply determined by the balance laws and jump conditions but by a kinetic relation.

(a) Albite twinned crystal) (b) Backlit twinned Selenite crystal

Figure 2.1: Twinning Models

2.3 Sharp Interface Theory

We introduce a continuum model for deformation twinning in single crystals in [3]. Sharp interface theory is used in this section, and more about its application has expanding to study micro-structural features such as particle translation, equilibrium shapes, shape bifurcations and particle growth [4–13].

The dynamics of twin growth is quasi-steady, thus allowing for transient effects and twin boundary shape changes that are slow compared to the average growth speed. Twinning deformation is described as an anti-plane shear deformation with

discontinuous strains, governed by an elastic potential with multiple wells. [14] The non-linear elastic constitutive law is proposed for body-centered cubic (BCC) crystals. The stored energy function possesses multiple potential wells and embodies unstable regimes of shear associated with a failure of ellipticity. [14] The structure of the mechanical response for anti-plane shear deformations is deduced from considerations of lattice symmetry. [14] Large, discontinuous shear strains localized within narrow twin lamellae are demonstrated in homogeneous equilibrium deformations of this material. The regions have a shape restricted by metastability. Their boundaries must be closely aligned with special composition planes, perform small curvature and terminate in cusps, [15] Hence, predicted needle-like configuration is in agreement with observed twin morphology. [16] The normal velocity of the twin boundary is always subsonic. In [17], it describes the dynamic anti-plane shear in three-dimension.

Our model is a specific one from [3]. We apply it in one-dimensional isotropic bar with two-wells stored-energy $\psi(\varepsilon)$ and constant density ρ in domain $\Omega \subset \mathbb{R}$. The displacement field $u(x,t)$ for $x \in \Omega$, $t \geq 0$, and it is assumed continuous and piece-wise smooth. The strain ε

$$\varepsilon = \nabla u = u_x \tag{2.1}$$

Form the constitutive relation of a hyperelastic material, the nominal stress is as the gradient of the stored-energy $\psi(\varepsilon)$

$$\sigma = \frac{\partial \psi}{\partial \varepsilon} \tag{2.2}$$

The two-well potential

$$\psi(\varepsilon) \geq \psi(\xi) = \psi(0) \qquad \text{for all} \quad \varepsilon \in \mathbb{R} \tag{2.3}$$

with global minimum wells at $\varepsilon = 0$ and ξ, where ξ is constant. Define the two disjoint regions as high-strain phase S^+ in subdomain Ω^+ and low-strain phase S^- in subdomain Ω^-, respectively and $\Omega = \Omega^+ \cup \Omega^-$, the subdomains evolve and change shapes in time according to the steady-state evolution in the model.

$$\sigma(\varepsilon) = \begin{cases} \sigma^+(\varepsilon) & \text{for} \quad \varepsilon \in S^+ \\ \sigma^-(\varepsilon) & \text{for} \quad \varepsilon \in S^- \end{cases} \tag{2.4}$$

Many problems in science and engineering contain evolving boundaries or interfaces and level set method is applies to solve these problems. Level set method was first proposed to represent these boundaries implicitly and model their propagation using appropriate partial differential equations by James A. Sethian and Stanley Osher in 1988 [18]. The boundaries are set as level set of function $\phi(\mathbf{x})$. In the sharp interface theory, the interfaces are treated as discontinuity surfaces of zeros thickness. The level set function $\phi = 0$ separates the whole domain Ω into two

sub-domains Ω^+ containing high strain phase and Ω^- containing low strain phase.

$$\phi \begin{cases} < 0 & \text{in} \quad \Omega^+ \\ = 0 & \text{in} \quad \Gamma_t \\ > 0 & \text{in} \quad \Omega^- \end{cases} \tag{2.5}$$

Details of these functions emerged crystallographic and material characteristics are referred to [14]. Strain and velocity discontinuities occur across the interface or twin boundary $\Gamma_t = \Omega^+ \cap \Omega^-$ obey the jump conditions [3],

$$[\![u_t]\!] + V[\![\nabla u]\!] = 0 \tag{2.6}$$

here, the jump is defined as $[\![\gamma]\!] = \gamma^+ - \gamma^-$ for any field γ across Γ_t. The jump of the momentum balance law on the interface is [3]

$$\rho V[\![u_t]\!] + [\![\sigma]\!] = 0 \qquad \Gamma_t \tag{2.7}$$

The shock waves are subject to the above jump conditions (2.6) and (2.7). However, strains on either side of a shock wave are in the same phase. The momentum equation in the bulk is

$$\nabla \cdot \sigma = \rho u_{tt} \quad \Omega - \Gamma_t \tag{2.8}$$

The motion of shock waves and interfaces consist energy dissipation. The rate of energy dissipation $D(t)$ is the excess of the rate of external work over the rate of change of stored elastic and kinetic energy and it is required to be nonnegative by the second thermodynamics law [19].

$$D_\Gamma = \int_{\partial\Omega} u_t \sigma n ds - \frac{d}{dt} \int_\Omega \left(\psi + \frac{1}{2} \rho u_t^2 \right) dA \geq 0 \tag{2.9}$$

[19] shows

$$D_\Gamma = \int_{\Gamma_t} gV ds \tag{2.10}$$

where V is the interface front velocity g is the driving force or configuration force on the moving interface Γ_t.

$$g = [\![C_k]\!], \quad C_k = \rho(\psi + k_{rel}) - \varepsilon : \sigma \tag{2.11}$$

Notice here from left to right, the strain phase is from high-strain phase in Ω^+ to low strain phase Ω^-. where C_k is the kinetic Eshellby tensor or energy-momentum tensor, $k_{rel} = \frac{1}{2}V^2$. Then, we can get

$$g = [\![\psi]\!] - \frac{1}{2}[\![\nabla u]\!] \left(\sigma^+ + \sigma^- \right) \tag{2.12}$$

The evolution of twin interfaces can not be governed only by field equations and Rankine-Hugoniot jump conditions of momentum balance. Therefore, a kinetic relation has to be introduced. A nucleation criterion is introduce which signals

the first occurrence of the phase change. From large study, it is found that the kinetic relation and the nucleation criterion together single out a unique solution to the Riemann problem with a special elastic material with a piecewise-linear, non-momotonic stress-strain relation. [20] This is suitable for one-dimensional problems or for isotropic materials. [3]

$$V = f(g) \quad \text{on} \quad \Gamma_t \tag{2.13}$$

Where f is the kinetic response function characteristic of the material between the driving force g and interface normal velocity V. To be consistent with the dissipation inequality, the function f must satisfy the dissipation inequality [19]

$$g \cdot f(g) \geq 0 \tag{2.14}$$

2.4 A Specific Model for Twinning

We choose the specific model for twinning in [1]. The stored energy is

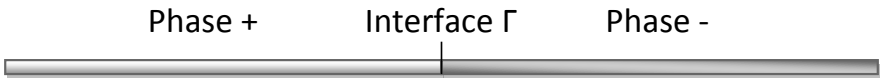

Figure 2.2: Rubber band with phase changing

$$\psi(\varepsilon) = \begin{cases} \frac{1}{2}\mu(\varepsilon - \xi)^2 & \text{for} \quad \varepsilon \in S^+ \quad \text{on} \quad \Omega_t^+ \\ \frac{1}{2}\mu\varepsilon^2 & \text{for} \quad \varepsilon \in S^- \quad \text{on} \quad \Omega_t^- \end{cases} \tag{2.15}$$

where $\mu > 0$ is the shear modulus. Then the stress-strain relation can be conducted by (2.2) and linear in each phase.

$$\sigma(\varepsilon) = \begin{cases} \mu(\varepsilon - \xi) & \text{for} \quad \text{on} \quad \Omega_t^+ \\ \mu\varepsilon & \text{for} \quad \text{on} \quad \Omega_t^- \end{cases} \tag{2.16}$$

Then (2.8) reduces to the wave equation

$$\triangle u = \frac{1}{c^2} u_{tt} \quad \text{on} \quad \Omega - \Gamma_t \tag{2.17}$$

where the shear wave speed $c = \sqrt{\mu/\rho}$. Combining (2.17) with jump conditions (2.6)(2.7), we get

$$[\![\nabla u]\!] = \frac{\xi}{1 - \frac{V^2}{c^2}} \tag{2.18}$$

This dictates the relation between the strain jump across Γ_t and the normal velocity V. If this applied to the same material, we can get

$$\frac{V^2}{c^2}[\![\nabla u]\!] = [\![\nabla u]\!] \tag{2.19}$$

This means the normal velocity must equal to the shear wave speed. This means that the shear shock waves reduce to the elastic shear waves in each phase.

The driving force in each phase is zero because the linearity of the stress-strain response. Then, the elastic waves in each phase are dissipation free. However, in general, the driving force on the twin interface does not vanish, (2.12) becomes

$$g = \frac{1}{2}\mu\xi(\varepsilon^+ + \varepsilon^- - \xi) \quad \text{on} \quad \Gamma_t \tag{2.20}$$

A specific form of the kinetic relation (2.13) for isotropic materials was considered [3]

$$V = f(g) = Mg \tag{2.21}$$

In above, we conduct the sharp-interface dynamic problem with (2.17) in the bulk and jump conditions (2.18) on the interface Γ_t. The evolution of Γ_t is determined by the kinetic relation (2.21), with g applied by (2.20). We give the initial conditions as

$$u(x,0) = u_0(x), \quad u_t(x,0) = v_0 \quad \text{for} \quad x \in \Omega; \quad \Gamma(t=0) = \Gamma_0 \tag{2.22}$$

and boundary conditions

$$u(0,t) = 0, \quad u(L,t) = kL \quad \text{in the perpendicular direction to} \quad x \tag{2.23}$$

where k is constant.

2.5 Diffuse Interface Theory

The sharp interface theory has an advantage that the system can be reformulated as boundary integral equations for which very efficient numerical methods have been developed. However, it is difficult to treat problems with mathematical singularities form when particles vanish, merge or split. Therefore, the diffuse interface (DI) theory can handle topological changes. [21–25] have shown its study in the effect of elastic fields on spiral decomposition, precipitating shapes and motions, and shape transitions such as particle splitting and merging.

In diffuse interface model, the sharp interface Γ_t is replaced by a narrow diffuse layer of specific thickness l_c across which all quantities are assumed to vary smoothly. Outside this layer, the field equations are the same with the sharp interface model.

The thickness l_c can not be arbitrary. It was observed that an apparent loss of mass occurs when the interface thickness is comparable to the length scale. [26] In views of accuracy and mass conservation, a thin interface is desirable in simulations. In principle, the thinner the interface thickness, the more accurate the numerical results. To reach a balance between the computational costs and interface resolution, the technique of adaptive grid refinement can be considered. [27, 28]

A dual-resolution Cartesian grid was proposed in [29]. The dual-resolution grids method is to apply finer resolution to the diffuse region and it can significantly increase the resolution of the interface with only a slight increase of the computational cost. Numerical results show that the dual-resolution grid save nearly

70% of the computational time in two-dimensional simulation and 80% in three-dimensional simulations and produces nearly the same results as the single-resolution grid [29]. We may utilize this dual-resolution grid if we investigate our problem in two-dimensional or three dimensional in the future.

The level set function ϕ separates the whole domain Ω into two sub-domains Ω^+ containing high strain phase and Ω^- containing low strain phase. respectively.

$$\phi \begin{cases} < 0 \quad \text{in} \quad \Omega^+ \\ = (x - l_a)/l_c \quad \text{in} \quad \Gamma_t \\ > 1 \quad \text{in} \quad \Omega^- \end{cases} \tag{2.24}$$

where l_a is the start point of the interface, l_b is the end of the interface, l_c is the thickness of the interface and the diffuse interface is a function with respect to time.

$$\Gamma_t = \{x \in [l_a, l_b] : \phi(x, t) = [0, 1]\} \tag{2.25}$$

The level set function $\phi(x, t)$ moving with normal velocity V obeys the Hamilton-Jacobi equation

$$\phi_t - V|\nabla\phi| = 0 \tag{2.26}$$

The diffuse layer is based on open phase using the phase-field variable $d(\phi) \in [0, 1]$, as a explicit function of ϕ . We choose the function $d(\phi)$ as

$$d(\phi) = \begin{cases} 1, & \phi < 0 \\ 1 - \phi + \frac{sin(2\pi\phi)}{2\pi}, & \phi \in [0, 1] \\ 0, & \phi > 1 \end{cases} \tag{2.27}$$

In 1D, we can apply the level set function as

$$\phi(x, t) = (x - \Gamma_t^f)/l_c \tag{2.28}$$

where the interface front position Γ_t^f at time t,

$$\Gamma_t^f = \Gamma_0 + \int_0^t V d\tau \tag{2.29}$$

We can prove that this level set function satisfy the Hamilton-Jacobi equation (2.26).

Across the diffuse layer, the strain phase gradually change from the low strain phase to the high strain phase, determining by the parameter $d(\phi)$. The diffuse interface transform the singular surface forces into continuous body forces localized in the interface region. [30] Then, the stored energy in this layer is

$$\psi = (1 - d(\phi))\psi^- + d(\phi)\psi^+ \tag{2.30}$$

Applying (2.2), the stress is gained as

$$\sigma = \mu(\varepsilon - d(\phi)\xi) \tag{2.31}$$

Applying the (2.17), the wave equation becomes as follows in this diffuse layer

$$\triangle u - \frac{d'(\phi)}{l_c} = \frac{1}{c^2} u_{tt} \quad \text{on} \quad \Gamma_t \tag{2.32}$$

Define the regularized driving force g as

$$g = -\frac{\partial \psi}{\partial d(\phi)} = \mu\xi(\varepsilon - \frac{1}{2}\xi) \tag{2.33}$$

Compared to the driving force (2.20) in sharp interface theory, the driving force calculated in (2.33) in DI method converges to the sharp interface model when the thickness l_c vanishes.

After the calculation of the configurational force, we can get the normal velocity V by (2.21). Finally, the problem in the diffuse interface is solved.

2.6 Arbitrary Lagrangian Eulerian methods

In solid mechanics, the Lagrangian description is fond of, in which the embedded mesh moves with the material thus, the convective effects is absent compared to the Eulerian approach. However, problems involving certain contact boundaries, especially those with sharp edges or corners, or emerged boundary conditions, especially a sharp jump, are difficult utilizing purely Lagrangian or purely Eulerian descriptions. Thus, the Arbitrary Lagrangian Eulerian (ALE) or mixed Lagrangian-Eulerian methods have been investigated. ALE methods were originally developed by Noh [31], Trulio [32] and Hirt, Amsden and Cook [33] in finite difference formats. The theoretical framework for ALE finite element descriptions has been established by Hughes, Liu, Zimmermann [34] in context of incompressible, viscous flows. Belytschko [35, 36] and Donea [37] proposed the ALE finite element methods for compressible, inviscid flows. Later, more work has been done [38–41].

More recently, ALE method is applied to properly account for the convection of information as the domain boundary evolves in flow problems with moving domains [42]. More specially, it utilizes the standard ALE method but "re-meshing" at each time step in order to always use the same given mesh, which discretizes the whole domain where the flow takes place. In [43], the filament-in-soap film problem found in the experimental model [44] is simulated by a fluid-structure interaction finite element method as a two-dimensional version of a flag-in-wind problem, where Navier-Stokes equations based on the interface-tracking ALE finite element method are coupled with the Lagrangian equilibrium equations of the structure. We can follow these ideas to use ALE method and re-meshing at each time step in our problem.

Arbitrary Lagrangian Eulerian (ALE) descriptions are arbitrary combinations of the Lagrangian and Eulerian descriptions. The prominent merit of ALE is the customized combination through the selection of mesh motion. ALE finite element formulations are to capture the benefits of both Lagrangian and Eulerian finite elements while minimizing the drawbacks.

The ALE formulation adds a convection term in the momentum equations. Non-physically oscillation may occur to solve the momentum equations containing convection terms applying the standard Galerkin Finite Element method [40]. The Streamline Upwind Petrov-Galerkin (SUPG) finite element method is proposed for convection domain flows with particular emphasis on the incompressible Navier-Stokes Equations in [45] and high accuracy are demonstrated. Later, in [46], more study is performed in SUPG employing to formulate the ALE finite element equations and several numerical examples have been solved and the numerical results indicate the effectiveness. More specially, the results of the one-dimensional wave propagation problem shows that SUPG method eliminates the unrealistic spatial oscillations completely while standard Galerkin method exhibits these oscillations. There are also other finite element methods, such as Galerkin Least Squares (GLS), Finite Increment calculus (FIC), which finally will be identical in the discretized formulation to SUPG if higher order omitted. [47] More details about ALE will be discussed in Chapter 3.

The solution above is fully coupled solution, which has been used in the work of subassembly simulation by T. Belytschko and J. M. Kennedy [48], fluid structure interaction by W.K.Liu [49], incompressible viscous flows by T. J. R. Hughes, W. K. Liu, and T. K. Zimmermann [50], viscous flow with large free surface motion by A. Huerta and W. K. Liu [51], interaction of fluid and a rigid body by T. Nomura and T. J. R. Hughes [52], incompressible hyperelasticity problem by T. Yamada and F. Kikuchi [53], and more recently in the work of incompressible Navier Strokes problems [54] and fluid structure interaction [55] by W. A. Wall and E. Ramm.

In 2003, a new ALE finite element formulation for strain plasticity in non-linear solid mechanics was proposed by Francisco Armero and Edward Love [56]. This new method decouples the governing equations and splits into a smoothing phase, an advection phase and a Lagrangian phase. The staggered approach leads to an efficient implementation of these methods, with a sequential solution of these motions. In classical ALE methods, difficulties lie in the numerical approximation of the advective terms and special devised schemes must be used to solve the governing equations. In contrast, this new method considers the direct interpolation of the motion of the material with respect to the reference mesh together with the motion of the spatial mesh with respect to this same reference mesh. This aspect is shown to be crucial for a simple treatment of the advection of the plastic internal variables and dynamic variables. Another advantage of this new method is that the calculation of the advection by carrying out through a particle tracking in the reference mesh can be accomplished very efficiently with the use of the connectivity graph of the fixed reference mesh. In addition, the access to the material mesh defined by the material map, besides the standard spatial mesh, allows to visualize clearly the limitation of the ALE formulations. In this approach,the measure of distortion of either material and spatial mesh is readily available, allowing a direct control of the smoothing process. This direct control is another merit over the classical ALE methods. In the future, we can use this method when expanding to strain plasticity problem.

2.7 Explicit Time Integration

Next, we need a suitable time integration method for our dynamics problem. Time integration methods are categorized into explicit methods, implicit methods, and semi-explicit methods. [57] Though implicit methods are unconditional stable and have high accuracy, they need an effective matrix and more than one time iterations per time step. Because our complex constitute law and high cost to use implicit time integration methods in updating meshes, only explicit methods are considered. The mainly common explicit methods are central difference methods, Runge-Kutta methods, stiffly stable methods, Predictor-Corrector (PC) methods and Taylor series schemes. The second order central difference explicit method is commonly used and is said to have the highest accuracy and maximum stability limit for any explicit method of order two [58].

The fourth order Runge-Kutta method have high accuracy, as the name suggested, however, it requires small time step, thus leading to slow convergence. An adaptive Runge-Kutta method [59] with optimized stability properties is not better than the explicit central difference [60]. For stiffly stable methods, it is difficulty with two offsetting factors: firstly, if small time steps are employed to accurately treat the stiff components, then the local computational time becomes excessive, and secondly, large time steps often result in instabilities and inaccurate response predictions. [61] AMPC (Adams Molton PC) is a second order AMPC scheme, but it takes long time to converge, While PEC (Predict Evaluate Correct) is more accurate than the fourth order Runge-Kutta method, but error estimation remain difficult. Taylor Series Schemes, based on Taylor series, are not desirable because its stability limit, though high accuracy can be gained. Experience has shown that the maximum time step is often dictated by the stability limit and not by the accuracy requirements. [62] The only advantage of the Taylor series over the central difference scheme would be an improved accuracy at the expense of an increase of computational effort. However, this advantage is not guaranteed for nonlinear problems [62].

Among these explicit methods, the central difference method is preferred and possesses no numerical dissipation for linear finite element discretization with a diagonal mass matrix and has period elongation behavior in one-dimensional case [63]. Fujii [64] has proved the convergence of a diagonal mass approximation. In computational aspects, the only disadvantage of these methods is that the time step must be small enough to be consistent with the numerical stability limits. The errors introduced by the lumped masses and the central difference scheme tend to be compensatory [65]. Therefore, central difference method using lumped mass is desirable both for accuracy and computational efficiency. Studies on its stability conducted for linear [58, 64, 66–68] and nonlinear problems [69, 70], and considering homogeneous strain elements [71, 72] show that the time step is limited for

$$\triangle t \leq \triangle t_{cr}, \quad \triangle t_{cr} \leq h/c \tag{2.34}$$

where h is the element length and c is the wave speed. The central difference method

update the displacement as follows [73].

$$u^{n+1,p} = u^n + \triangle t v^n + \frac{(\triangle t)^2}{2} a^n \tag{2.35}$$

$$v^{n+1,p} = v^n + \frac{\triangle t}{2} a^n \tag{2.36}$$

$$u^{n+1} = u^{n+1,p} \tag{2.37}$$

$$v^{n+1} = v^{n+1,p} + \frac{\triangle t}{2} a^{n+1} \tag{2.38}$$

where the signal n or $n+1$ represents the time step, u is the displacement, v is the material velocity and a is the material acceleration.

Chapter 3

Arbitrary Lagrangian Eulerian formulations

3.1 Preliminaries

Define the initial domain Ω_0, the current or spatial domain Ω, and the referential or ALE domain $\hat{\Omega}$. The motion of material is described as

$$\mathbf{x} = \boldsymbol{\eta}(\mathbf{X}, t) \tag{3.1}$$

Where X are the material coordinate and function $\eta(X, t)$ is mapping from the initial domain Ω_0 to the current domain Ω for each time t. The motion of mesh is described as

$$\mathbf{x} = \boldsymbol{\zeta}(\boldsymbol{\chi}, t) \tag{3.2}$$

Where χ is the referential or ALE coordinates and function $\hat{\phi}(\chi, t)$ is mapping from the referential domain $\hat{\Omega}$ to the current domain Ω. Combining (3.1) and (3.2), the map from the material coordinates to the ALE coordinates is a function of time.

$$\boldsymbol{\chi} = \boldsymbol{\zeta}^{-1}(x, t) = \hat{\boldsymbol{\zeta}}^{-1}(\boldsymbol{\eta}(\mathbf{X}, t), t) = \boldsymbol{\theta}(X, t) \tag{3.3}$$

The maps between material configuration, reference configuration and spatial configuration are show in Fig.3.1

The classical or material displacement u, velocity v and acceleration a are respectively defined by

$$\mathbf{u} = \mathbf{x} - \mathbf{X} \tag{3.4}$$

$$\mathbf{v} = \frac{\partial \mathbf{u}}{\partial t}|_{\mathbf{X}} \tag{3.5}$$

$$\mathbf{a} = \frac{\partial \mathbf{v}}{\partial t}|_{\mathbf{X}} = \mathbf{u}_{,tt[\mathbf{X}]} \tag{3.6}$$

In ALE algorithm, analogously we define the displacement, velocity and acceleration of the mesh motion, which will be called the mesh displacement $\hat{\mathbf{u}}$, mesh velocity $\hat{\mathbf{v}}$ and mesh acceleration $\hat{\mathbf{a}}$.

$$\hat{\mathbf{u}} = \mathbf{x} - \boldsymbol{\chi} \tag{3.7}$$

$$\hat{\mathbf{v}} = \frac{\partial \hat{\mathbf{u}}}{\partial t}|_{\boldsymbol{\chi}} \tag{3.8}$$

$$\hat{\mathbf{a}} = \frac{\partial \hat{\mathbf{v}}}{\partial t}|_{\boldsymbol{\chi}} = \hat{\mathbf{u}}_{,tt[\boldsymbol{\chi}]} \tag{3.9}$$

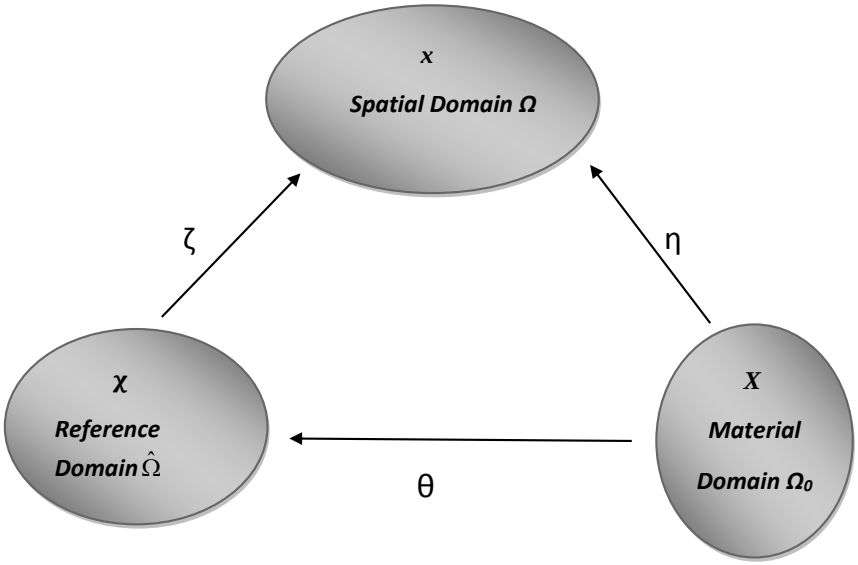

Figure 3.1: ALE descriptions

We finish the preliminary definitions for our ALE descriptions. Actually, the Lagrangian description used mostly in solid and Eulerian description used most in fluid are special ALE descriptions, shown in Tab. 3.1. When the referential domain is identical to the material domain,$\boldsymbol{\chi} = \mathbf{X}$, we get the Lagrangian description, shown in Fig.3.2. When the referential domain is identical to the spatial domain,$\boldsymbol{\chi} = \mathbf{x}$, we get the Eulerian description,shown in Fig.3.3.

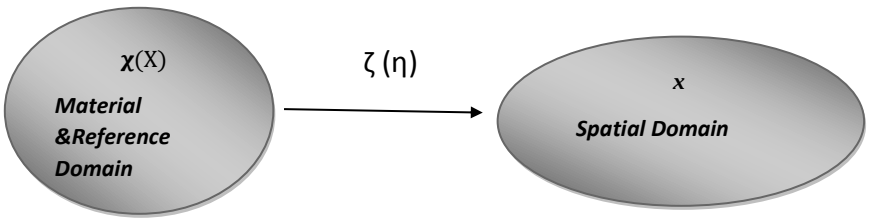

Figure 3.2: Lagrangian Description

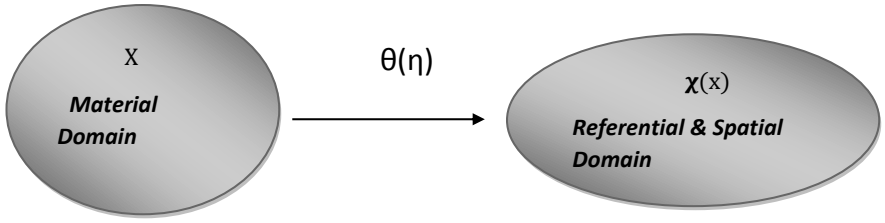

Figure 3.3: Eulerian Description

Description		General ALE	Lagrangian	Eulerian
Motion	Material	$\mathbf{x} = \boldsymbol{\eta}(\mathbf{X}, t)$	$\mathbf{x} = \boldsymbol{\eta}(\mathbf{X}, t)$	$\mathbf{x} = \boldsymbol{\eta}(\mathbf{X}, t)$
	Mesh	$\mathbf{x} = \boldsymbol{\zeta}(\boldsymbol{\chi}, t)$	$\mathbf{x} = \boldsymbol{\eta}(\mathbf{X}, t)$	$\mathbf{x} = \mathbf{I}(\mathbf{x})$
			$(\boldsymbol{\chi} = \mathbf{X}, \boldsymbol{\zeta} = \boldsymbol{\eta})$	$(\boldsymbol{\chi} = \mathbf{x}, \boldsymbol{\zeta} = \mathbf{I})$
Displacement	Material	$\mathbf{u} = \mathbf{x} - \mathbf{X}$	$\mathbf{u} = \mathbf{x} - \mathbf{X}$	$\mathbf{u} = \mathbf{x} - \mathbf{X}$
	Mesh	$\hat{\mathbf{u}} = \mathbf{x} - \boldsymbol{\chi}$	$\hat{\mathbf{u}} = \mathbf{x} - \mathbf{X} = \mathbf{u}$	$\hat{\mathbf{u}} = \mathbf{x} - \mathbf{x} = 0$
Velocity	Material	$\mathbf{v} = \mathbf{u}_{,t[\mathbf{X}]}$	$\mathbf{v} = \mathbf{u}_{,t[\mathbf{X}]}$	$\mathbf{v} = \mathbf{u}_{,t[\mathbf{X}]}$
	Mesh	$\hat{\mathbf{v}} = \hat{\mathbf{u}}_{,t[\boldsymbol{\chi}]}$	$\hat{\mathbf{v}} = \hat{\mathbf{u}}_{,t[\mathbf{X}]} = \mathbf{v}$	$\hat{\mathbf{v}} = \hat{\mathbf{u}}_{,t[\mathbf{X}]} = 0$
Acceleration	Material	$\mathbf{a} = \mathbf{v}_{,t[\mathbf{X}]}$	$\mathbf{a} = \mathbf{v}_{,t[\mathbf{X}]}$	$\mathbf{a} = \mathbf{v}_{,t[\mathbf{X}]}$
	Mesh	$\hat{\mathbf{a}} = \hat{\mathbf{v}}_{,t[\boldsymbol{\chi}]}$	$\hat{\mathbf{a}} = \hat{\mathbf{v}}_{,t[\mathbf{X}]} = \mathbf{a}$	$\hat{\mathbf{a}} = \hat{\mathbf{v}}_{,t[\mathbf{X}]} = 0$

Note: $\mathbf{I}$ is the identity tensor

Table 3.1: Comparison of the kinematics for an ALE formulation with purely Lagrangian and purely Eulerian descriptions

3.2 Time derivative

Considering a specific function f, the material time derivative can be expressed for the different descriptions as follows:

$$\frac{Df}{Dt} = \dot{f} = \frac{\partial f(\mathbf{X}, t)}{\partial t} \qquad \text{Lagrangian description} \quad (\mathbf{X}, t) \tag{3.10}$$

$$= f_{,t[x]} + \frac{\partial f}{\partial x_i}\frac{\partial x_i}{\partial t}_{[X]} \qquad \text{Eulerian description} \quad (\mathbf{x}, t) \tag{3.11}$$

$$= f_{,t[\chi]} + \frac{\partial f}{\partial \chi_i}\frac{\partial \chi_i}{\partial t}_{[X]} \qquad \text{ALE description} \quad (\boldsymbol{\chi}, t) \tag{3.12}$$

The referential particle velocity $\mathbf{w}$ is the particle velocity as seen from the referential domain $\hat{\Omega}$, since it measures the time variation of the referential coordinate $\boldsymbol{\chi}$ holding the material particle $\mathbf{X}$ fixed. It's defined by

$$\mathbf{w} = \frac{\partial \boldsymbol{\chi}}{\partial t}_{[X]} \tag{3.13}$$

Define the convective velocity between the material and the mesh $\mathbf{c}$, which is the particle velocity relative to the mesh as seen from the spatial domain Ω.

$$\mathbf{c} = \mathbf{v} - \hat{\mathbf{v}} \tag{3.14}$$

Applying the mapping connection (3.3), the material velocity gives

$$v_j = \frac{\partial \eta_j(\mathbf{X},t)}{\partial t} = \frac{\partial \zeta_j(\boldsymbol{\chi},t)}{\partial t} + \frac{\partial \zeta_j(\boldsymbol{\chi},t)}{\partial \chi_j}\frac{\partial \theta j(\mathbf{X},t)}{\partial t} = \hat{v}_j + \frac{\partial x_j}{\partial \chi_j}\frac{\partial \chi_j}{\partial t}|_{\mathbf{X}} \tag{3.15}$$

Combining (3.14) and (3.15), the connection between the referential particle velocity $\mathbf{w}$ and the convective velocity $\mathbf{c}$ can be demonstrated

$$\mathbf{c} = \frac{\partial \mathbf{x}}{\partial \boldsymbol{\chi}}\frac{\partial \boldsymbol{\chi}}{\partial t}|_{\mathbf{X}} = \frac{\partial \mathbf{x}}{\partial \boldsymbol{\chi}}\mathbf{w} \tag{3.16}$$

(3.16) implies that $\mathbf{c} = \mathbf{w}$ if and only if $\frac{\partial \mathbf{x}}{\partial \boldsymbol{\chi}} = \mathbf{I}$, that is, when the mesh motion is purely transient, without rotations or deformations of any kind. In our small strain and relatively slow phase changing problem, where $\frac{\partial \mathbf{x}}{\partial \boldsymbol{\chi}} = \mathbf{I}$ can be an approximation, we apply this approximation $\mathbf{c} = \mathbf{w}$.

Using (3.16) the time derivative become

$$\frac{Df}{Dt} = \dot{f} = f_{,t[\chi]} + \frac{\partial f}{\partial \chi_i}\frac{\partial \chi_i}{\partial t}_{[X]} = f_{,t[\chi]} + \frac{\partial f}{\partial x_i}\frac{\partial x_i}{\partial \chi_j}w_j \tag{3.17}$$

or

$$\frac{Df}{Dt} = \dot{f} = f_{,t[\chi]} + \frac{\partial f}{\partial \chi_i}w_i = f_{,t[\chi]} + \frac{\partial f}{\partial x_i}c_i \tag{3.18}$$

3.3 Lagrangian finite element formulations

3.3.1 Governing equations

In solid mechanics,Lagrangian meshes are most popular as it is easy to handle complicated boundaries and fixed with material points, so that historical dependent materials can be treated accurately. The conservation laws in Lagrangian description are

$$\text{Mass: } \dot{\rho} = -\rho v_{j,j} \tag{3.19}$$

$$\text{Momentum: } \rho \dot{v}_i = \sigma_{ji,j} + \rho b_i \tag{3.20}$$

$$\text{Internal Energy: } \rho \dot{E} = (\sigma_{ij} v_i)_{,j} + b_i v_i \tag{3.21}$$

where ρ is the mass density, $\mathbf{v}$ is the material velocity vector, $\boldsymbol{\sigma}$ is the Cauchy stress tensor, $\mathbf{b}$ is the specific body force vector and E is the specific total energy. Only mechanical energies are considered in the above form of the energy equation. The Cauchy stress tensor $\boldsymbol{\sigma}$ is assumed identical to the first Piola Kirchhoff stress tensor P in small strain problem.

A common assumption of taking the density ρ as constant, so that the mass conservation (3.19) reduces to

$$v_{j,j} = 0 \tag{3.22}$$

This is the well know incompressibility condition, which leave us only to solve the momentum conservation equation. This simplification is also commonly neglected

in solid mechanics because elastic deformation typically induce very small changes in volume while plastic deformations are volume preserving. That is the changes in density are negligible and the mass conservation (3.19) automatically holds to sufficient approximation with no need to add it to the set of governing equations.

3.3.2 Weak form

Now we focus on the momentum equation (3.20) and use standard Galerkin Finite Element method with Lagrangian mesh. The strong form consists of momentum balance the traction boundary conditions and traction continuity conditions.

$$\rho \dot{v}_i = \sigma_{ji,j} + \rho b_i \text{ in } \Omega \tag{3.23}$$

$$\bar{t}_i = n_j \sigma_{ji} \text{ on } \Gamma_{ti} \tag{3.24}$$

$$[\![n_j \sigma_{ji}]\!] = 0 \text{ on } \Gamma_{int} \tag{3.25}$$

where Γ_{ti} is the traction boundary and Γ_{int} is the union of all surfaces on which the stress are discontinuous in the body.

Multiplying a test function u^* and integrating over the current domain Ω, we get

$$\int_\Omega u_i^* \rho \dot{v}_i d\Omega = \int_\Omega u_i^* \sigma_{ji,j} d\Omega + \int_\Omega u_i^* \rho b_i d\Omega \tag{3.26}$$

The first term in the right hand side can be next expanded by the product rule, which gives

$$\int_\Omega u_i^* \sigma_{ji,j} d\Omega = \int_\Omega \frac{\partial}{\partial x_j}(u_i^* \sigma_{ji}) d\Omega - \int_\Omega u_{i,j}^* \sigma_{ji} d\Omega \tag{3.27}$$

We assume that the discontinuities occur over a finite set of surfaces Γ_{int}, so Gauss's theorem gives

$$\int_\Omega \frac{\partial}{\partial x_j}(u_i^* \sigma_{ji}) d\Omega = \int_{\Gamma_{int}} u_i^* [\![n_j \sigma_{ji}]\!] d\Gamma + \int_\Gamma u_i^* n_j \sigma_{ji} d\Gamma \tag{3.28}$$

Using the boundary conditions in (3.3.2), this becomes

$$\int_\Omega \frac{\partial}{\partial x_j}(u_i^* \sigma_{ji}) d\Omega = \int_\Gamma u_i^* \bar{t}_i d\Gamma \tag{3.29}$$

Uniting (3.26) and (3.29) , we get the weak form for the momentum balance.

$$\int_\Omega u_i^* \rho \dot{v}_i d\Omega = -\int_\Omega u_{i,j}^* \sigma_{ji} d\Omega + \int_\Omega u_i^* \rho b_i d\Omega + \int_{\Gamma_t} u_i^* \bar{t}_i d\Gamma \tag{3.30}$$

3.3.3 Finite element discretization

After getting the weak form of momentum balance, the next step is to develop the discrete finite element equations.

Define the initial coordinates, material displacement, material velocity, material acceleration and test function, respectively, as functions of element coordinates.

The finite element approximations to the motion, displacement, material velocity, material acceleration are given by as follows respectively,

$$\mathbf{x}(\mathbf{X},t) = \mathbf{x}_I(t)N_I(\mathbf{X}) \tag{3.31}$$
$$\mathbf{u}(\mathbf{X},t) = \mathbf{u}_I(t)N_I(\mathbf{X}) \tag{3.32}$$
$$\mathbf{v}(\mathbf{X},t) = \mathbf{v}_I(t)N_I(\mathbf{X}) \tag{3.33}$$
$$\mathbf{a}(\mathbf{X},t) = \mathbf{a}_I(t)N_I(\mathbf{X}) \tag{3.34}$$

and the test functions are not functions of time, so

$$u^*(\mathbf{X}) = N_I(\mathbf{X}) \tag{3.35}$$

where the shape functions $N_I(\mathbf{X})$ are functions of the material or Lagrangian coordinates.

Substitute (3.3.3) to (3.35) into (3.30), we get the matrix formulation of the Lagrangian finite element method

$$\mathbf{Ma} = \mathbf{f}^{ext} - \mathbf{f}^{int} \tag{3.36}$$

where

$$\begin{aligned}
\mathbf{M} &= \mathbf{I}\left[M_{IJ}\right] = \left(\int_{\Omega_0} \rho_0 N_I N_J d\Omega_0\right)\mathbf{I} \\
\mathbf{f}^{int} &= \left[f_{iI}^{int}\right] = \int_{\Omega_0} N_{I,j}\sigma_{ij} d\Omega_0 \\
\mathbf{f}^{ext} &= \left[f_{iI}^{ext}\right] = \int_{\Omega_0} \rho N_I b_i d\Omega_0 + \int_{\Omega} \rho N_I \bar{t}_i d\Omega_0
\end{aligned} \tag{3.37}$$

3.4 Eulerian finite element formulations

In order to better understand ALE finite element method, we develop the Eulerian finite element formulations. Eulerian finite element method is also called updated Lagrangian finite element method.

The conservation laws in Eulerian description are

$$\text{Mass: } \rho_{,t[x]} + \rho_{,j}v_j = -\rho v_{j,j} \tag{3.38}$$
$$\text{Momentum: } \rho(v_{i,t[x]} + v_j v_{i,j}) = \sigma_{ji,j} + \rho b_i \tag{3.39}$$
$$\text{Internal Energy: } \rho(E_{,t[x]} + E_{,j}v_j) = (\sigma_{ij}v_i)_{,j} + b_i v_i \tag{3.40}$$

Analogously to Lagrangian method, we also focus on the momentum balance. Notice that from the time derivatives $\dot{v} = v_{i,t[x]} + v_j v_{i,j}$ and replacing 3.30 with $\dot{v} = v_{i,t[x]} + v_j v_{i,j}$, we can get the weak form for Eulerian method.

$$\int_{\Omega} u_i^* \rho(v_{i,t[x]} + v_j v_{i,j}) d\Omega = -\int_{\Omega} u_{i,j}^* \sigma_{ji} d\Omega + \int_{\Omega} u_i^* \rho b_i d\Omega + \int_{\Gamma_t} u_i^* \bar{t}_i d\Gamma \tag{3.41}$$

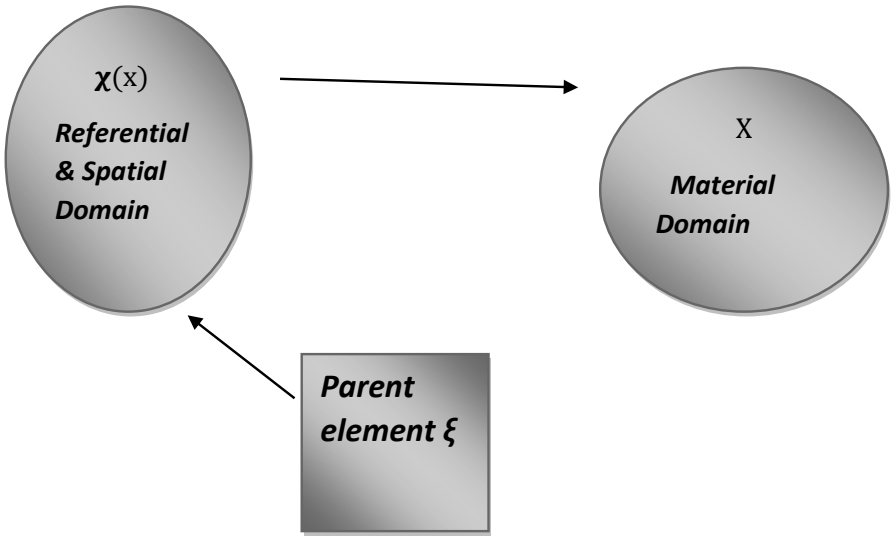

Figure 3.4: Material, spatial configurations and their relationship to the parent coordinate

We solve (3.41) within standard Galerkin Finite Element method. The connection of the material, spatial configurations and their relationship to the parent coordinate is shown in Fig. 3.4

Define the initial coordinates, material displacement, material velocity, material acceleration and test function, respectively, as functions of element coordinates.

$$\mathbf{x}(\boldsymbol{\xi}^e, t) = \mathbf{x}_I(t) N_I(\boldsymbol{\xi}^e) \tag{3.42}$$

$$\mathbf{u}(\boldsymbol{\xi}^e, t) = \mathbf{u}_I(t) N_I(\boldsymbol{\xi}^e) \tag{3.43}$$

$$\mathbf{v}(\boldsymbol{\xi}^e, t) = \mathbf{v}_I(t) N_I(\boldsymbol{\xi}^e) \tag{3.44}$$

$$\mathbf{a}(\boldsymbol{\xi}^e, t) = \mathbf{a}_I(t) N_I(\boldsymbol{\xi}^e) \tag{3.45}$$

$$u^* = u_I^* N_I(\boldsymbol{\xi}^e) \tag{3.46}$$

Substitute (3.42)-(3.46) into (3.41), we get

$$\mathbf{M}\mathbf{a} = \mathbf{f}^{ext} - \mathbf{f}^{int} \tag{3.47}$$

where

$$\begin{aligned} \mathbf{M} &= \mathbf{I}\left[M_{IJ}\right] = \left(\int_\Omega \rho N_I N_J d\Omega\right)\mathbf{I} \\ \mathbf{f}^{int} &= \left[f_{iI}^{int}\right] = \int_\Omega N_{I,j}\sigma_{ij} d\Omega \\ \mathbf{f}^{ext} &= \left[f_{iI}^{ext}\right] = \int_\Omega \rho N_I b_i d\Omega + \int_\Omega \rho N_I \bar{t}_i d\Omega \end{aligned} \tag{3.48}$$

3.5 ALE finite element formulations

We will use the conversation laws to develop the ALE finite element formulations.

Similar to Eulerian description, the conservation laws in ALE descriptions are

$$\text{Mass: } \rho_{,t[\chi]} + \rho_{,j} c_j = -\rho v_{j,j} \tag{3.49}$$

$$\text{Momentum: } \rho(v_{i,t[\chi]} + c_j v_{i,j}) = \sigma_{ji,j} + \rho b_i \tag{3.50}$$

$$\text{Internal Energy: } \rho(E_{,t[\chi]} + E_{,j} c_j) = (\sigma_{ij} v_i)_{,j} + b_i v_i \tag{3.51}$$

We consider transient problem with elastic material in small strain in the domain Ω bounded by $\partial\Omega$. The momentum equation is described in Eulerian as

$$\rho \dot{v}_i = \sigma_{ji,j} + \rho b_i \quad \text{in} \quad \Omega \tag{3.52}$$

Applying the material time derivative operator (3.18), the momentum equation becomes

$$\rho \left\{ v_{i,t[\chi]} + c_j v_{i,j} \right\} = \sigma_{ji,j} + \rho b_i \quad \text{in} \quad \Omega \tag{3.53}$$

The weak form of the momentum equation can be obtained by multiplying the strong form 3.52 by the test function u^* over the spatial domain Ω and employing the divergence theorem to imbibe the traction forces on the boundary $\partial\Omega$. This results

$$\int_\Omega u_i^* \rho \dot{v}_i d\Omega = -\int_\Omega u_{i,j}^* \sigma_{ji} d\Omega + \int_\Omega u_i^* \rho b_i d\Omega + \int_{\Gamma_t} u_i^* \bar{t}_i d\Gamma \tag{3.54}$$

Analogous to 3.53, we get

$$\int_\Omega u_i^* \rho v_{i,t[\chi]} d\Omega + \int_\Omega u_i^* \rho c_j v_{i,j} d\Omega = -\int_\Omega u_{i,j}^* \sigma_{ji} d\Omega + \int_\Omega u_i^* \rho b_i d\Omega + \int_{\Gamma_t} u_i^* \bar{t}_i d\Gamma \tag{3.55}$$

Where $\bar{t_i} = \sigma_{ij} n_j$ are the natural boundary conditions applied on Γ_t.

3.6 Streamline Upwind Petrov-Galerkin Method

Now we apply Streamline Upwind Petrov-Galerkin (SUPG) finite element method to solve the convection-diffusion problem (3.55). The connection of the material, reference, spatial configurations and their relationship to the parent coordinate is shown in Fig. 3.5

Define the variables ALE coordinates, mesh motion, material displacement, mesh velocity,mesh acceleration convection velocity and test function, respectively, as functions of element coordinates.

$$\boldsymbol{\chi}(\boldsymbol{\xi}^e) = \boldsymbol{\chi}_I N_I(\boldsymbol{\xi}^e) \tag{3.56}$$

$$\mathbf{x}(\boldsymbol{\xi}^e, t) = \mathbf{x}_I(t) N_I(\boldsymbol{\xi}^e) \tag{3.57}$$

$$\mathbf{u}(\boldsymbol{\xi}^e, t) = \mathbf{u}_I(t) N_I(\boldsymbol{\xi}^e) \tag{3.58}$$

$$\hat{\mathbf{v}}(\boldsymbol{\xi}^e, t) = \hat{\mathbf{v}}_I(t) N_I(\boldsymbol{\xi}^e) \tag{3.59}$$

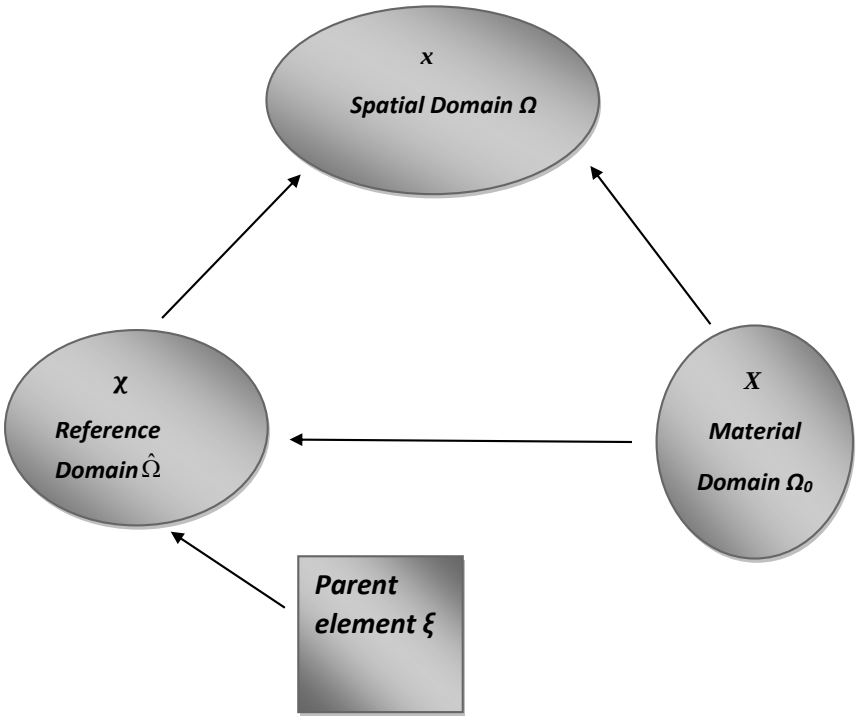

Figure 3.5: Material, spatial configurations and their relationship to the parent coordinate

$$\hat{\mathbf{a}}(\boldsymbol{\xi}^e, t) = \hat{\mathbf{a}}_I(t) N_I(\boldsymbol{\xi}^e) \tag{3.60}$$

$$\mathbf{c}(\boldsymbol{\xi}^e, t) = \mathbf{c}_I(t) N_I(\boldsymbol{\xi}^e) \tag{3.61}$$

$$u_i^* = N_i + N_i^{PG} \tag{3.62}$$

Where N is still the shape function, $N_i^{PG} = \tau c_j N_{i,j}$, $\tau = \| \alpha \| \frac{h}{2\|c\|}$ and h is the element length.

Applying the test function $u_i^* = N_i + N_i^{PG}$ into the weak form (3.55), we can get

$$\begin{aligned}\int_\Omega N_i \rho v_{i,t[\chi]} d\Omega + \int_\Omega N_i \rho c_j v_{i,j} d\Omega + \int_\Omega N_{i,j} \sigma_{ji} d\Omega - \int_\Omega N_i \rho b_i d\Omega - \int_{\Gamma_t} N_i \bar{t}_i d\Gamma \\ + \int_\Omega N_i^{PG} \left(\rho v_{i,t[\chi]} + \rho c_j v_{i,j} - \sigma_{ji,j} - \rho b_i \right) d\Omega = 0\end{aligned} \tag{3.63}$$

Introduction of (3.56)-(3.62) into (3.63) results in

$$(\mathbf{M} + \mathbf{M}_{stab}) \frac{d\hat{\mathbf{v}}}{dt} + (\mathbf{L} + \mathbf{L}_{stab}) \hat{\mathbf{v}} + (\mathbf{f}^{int} + \mathbf{f}_{stab}^{int}) = (\mathbf{f}^{ext} + \mathbf{f}_{stab}^{ext}) \tag{3.64}$$

where

$$\begin{aligned}
&\mathbf{M} = \mathbf{I}\,[M_{IJ}] = \left(\int_\Omega \rho N_I N_J d\Omega\right)\mathbf{I}, \quad \mathbf{M}_{stab} = \mathbf{I}\,[M_{IJ}]_{stab} = \left(\int_\Omega \rho\tau c_j N_{I,j} N_J d\Omega\right)\mathbf{I} \\
&\mathbf{L} = \mathbf{I}\,[L_{IJ}] = \left(\int_\Omega \rho N_I c_i N_{J,i} d\Omega\right)\mathbf{I}, \quad \mathbf{L}_{stab} = \left(\int_\Omega \rho\tau c_j N_{I,j} c_i N_{J,i} d\Omega\right)\mathbf{I} \\
&\mathbf{f}^{int} = \left[f_{iI}^{int}\right] = \int_\Omega N_{I,j}\sigma_{ij} d\Omega, \quad (\mathbf{f}^{int})_{stab} = -\int_\Omega \tau c_j N_{I,j}\sigma_{ki,k} d\Omega \\
&\mathbf{f}^{ext} = \left[f_{iI}^{ext}\right] = \int_\Omega \rho N_I b_i d\Omega + \int_\Omega \rho N_I \bar{t}_i d\Omega, \quad \mathbf{f}_{stab}^{ext} = \left[f_{iI}^{ext}\right]_{stab} = \int_\Omega \rho\tau c_j N_{I,j} b_i d\Omega
\end{aligned} \tag{3.65}$$

3.7 Mesh Update

The option of arbitrary is a great advantage of ALE, whereas this arbitrary makes us treat the mesh differently. In general, there are several ways, mesh motion prescribed a priori, Lagrangian Euler matrix method ref Hughes1981 and automatic mesh generation [73]. As for our problem, we treat it as mesh motion prescribed a priori.

As the interface moves in time and we know the interface velocity in advance, therefore, we assume that the mesh in the interface moves the same as the interface velocity governed by (2.21). To fixed in the domain, we fix the start and end point of the mesh. The convection velocity c is as follows,

$$c = \begin{cases} -w * x * (x - 2 * l_a)/(l_a)^2 \\ w \\ -w * (x - 1) * (x - 2 * l_b + 1)/(1 - l_b)^2 \end{cases} \tag{3.66}$$

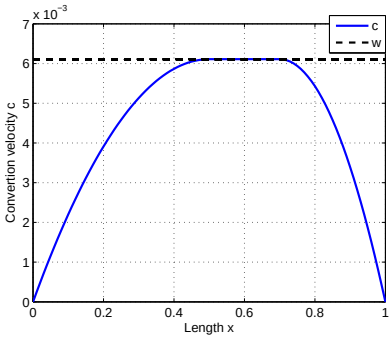

Figure 3.6: Convection velocity

3.8 Flowchart of the Numerical Implementation

3.8.1 Flowchart of Lagrangian finite elements methods

1. Update time:
   $t^{n+1} = t^n + \triangle t$

2. Compute the driving force at last time step t^n:
   Sharp interface theory:
   $g^n = \frac{1}{2}\mu\xi(\varepsilon^+ + \varepsilon^- - \xi)$
   Diffuse interface theory:
   $g^n = \int_0^{l_c} y d'(\phi) d\phi$

3. Compute interface velocity at last time step t^n:
   $w^n = Mg^n$

4. Update interface position:
   $\Gamma^{n+1} = \Gamma^n + w^n \triangle t$

5. Update predict displacement $\mathbf{u}^{n+1,p}$ and predict velocity $\mathbf{v}^{n+1,p}$
   $\mathbf{u}^{n+1,p} = \mathbf{u}^n + \triangle t \mathbf{v}^n + \frac{(\triangle t)^2}{2}\mathbf{a}^n$
   $\mathbf{v}^{n+1,p} = \mathbf{v}^n + \frac{\triangle t}{2}\mathbf{a}^n$

6. Compute predict strain $\boldsymbol{\varepsilon}^{n+1,p} = \nabla \mathbf{u}^{n+1,p}$ and predict stress $\boldsymbol{\sigma}^{n+1,p}$
   $\boldsymbol{\sigma}^{n+1,p} = f(\boldsymbol{\varepsilon}^{n+1,p})$

7. Solve matrix equation to get acceleration $\mathbf{a}^{n+1}$
   $\mathbf{M}\mathbf{a}^{n+1} = \mathbf{f}^{ext} - \mathbf{f}^{int}$

8. Update displacement $\mathbf{u}^{n+1}$ and velocity $\mathbf{v}^{n+1}$
   $\mathbf{u}^{n+1} = \mathbf{u}^{n+1,p}$
   $\mathbf{v}^{n+1} = \mathbf{v}^{n+1,p} + \frac{\triangle t}{2}\mathbf{a}^{n+1}$

9. Update strain $\boldsymbol{\varepsilon}^{n+1} = \nabla \mathbf{u}^{n+1}$ and stress $\boldsymbol{\sigma}^{n+1}$
   $\boldsymbol{\varepsilon}^{n+1} = \nabla \mathbf{u}^{n+1}$
   $\boldsymbol{\sigma}^{n+1} = f(\boldsymbol{\varepsilon}^{n+1})$

3.8.2 Flowchart of ALE finite elements methods

1. Update time:
   $t^{n+1} = t^n + \triangle t$

2. Compute the driving force at last time step t^n:
   Sharp interface theory:
   $g^n = \frac{1}{2}\mu\xi(\varepsilon^+ + \varepsilon^- - \xi)$
   Diffuse interface theory:
   $g^n = \int_0^{l_c} y d'(\phi) d\phi$

3. Compute interface velocity at last time step t^n:
   $w^n = Mg^n$

4. Update mesh, update convection velocity $\mathbf{c}$

5. Update matrix $\mathbf{M}$, $\mathbf{M}_{stab}$, $\mathbf{L}$, and $\mathbf{L}_{stab}$

6. Update predict displacement $\mathbf{u}^{n+1,p}$ and predict velocity $\mathbf{v}^{n+1,p}$
   $\mathbf{u}^{n+1,p} = \mathbf{u}^n + \triangle t\mathbf{v}^n + \frac{(\triangle t)^2}{2}\mathbf{a}^n$
   $\mathbf{v}^{n+1,p} = \mathbf{v}^n + \frac{\triangle t}{2}\mathbf{a}^n$

7. Compute predict strain $\boldsymbol{\varepsilon}^{n+1,p} = \nabla\mathbf{u}^{n+1,p}$ and predict stress $\boldsymbol{\sigma}^{n+1,p}$
   $\boldsymbol{\sigma}^{n+1,p} = f(\boldsymbol{\varepsilon}^{n+1,p})$

8. Solve matrix equation to get acceleration $\mathbf{a}^{n+1}$
   $(\mathbf{M} + \mathbf{M}_{stab})\frac{d\hat{\mathbf{v}}}{dt} + (\mathbf{L} + \mathbf{L}_{stab})\hat{\mathbf{v}} + (\mathbf{f}^{int} + \mathbf{f}^{int}_{stab}) = (\mathbf{f}^{ext} + \mathbf{f}^{ext}_{stab})$

9. Update displacement $\mathbf{u}^{n+1}$ and velocity $\mathbf{v}^{n+1}$
   $\mathbf{u}^{n+1} = \mathbf{u}^{n+1,p}$
   $\mathbf{v}^{n+1} = \mathbf{v}^{n+1,p} + \frac{\triangle t}{2}\mathbf{a}^{n+1}$

10. Update strain $\boldsymbol{\varepsilon}^{n+1} = \nabla\mathbf{u}^{n+1}$ and stress $\boldsymbol{\sigma}^{n+1}$
    $\boldsymbol{\varepsilon}^{n+1} = \nabla\mathbf{u}^{n+1}$
    $\boldsymbol{\sigma}^{n+1} = f(\boldsymbol{\varepsilon}^{n+1})$

Chapter 4

FiGALE Method

4.1 Thick Level Set

4.1.1 Introduction

Different from [1], Thick Level Set (TLS) is applied in our problem. TLS was first proposed to model damage growth in solid by Nicolas Moës in 2011 [74]. Fully damaged and undamaged zones are separated by a level set function ϕ, representing the damage variable. Beyond a critical length, the material is assumed to be totally damaged, thus allowing a straightforward transition to fracture. The configurational force driving the damage front is non-local in the sense that it averages over the thickness in the wake of the front.

We assume that the diffuse interface moves at the front velocity at particular time. Namely, the interface layer always moves together and maintains the same thickness. Following this, the configurational force g can be interpreted as a configurational force per unit length on the front.

$$g(s) = \int_0^{l_c} y(\phi, s) d'(\phi) \left(1 - \frac{\phi}{\rho(s)}\right) d\phi \tag{4.1}$$

where the configurational force is an average of the local driving force y weighed by $d(\phi)$, the evolution of the front curvature $\rho(s)$ along the thickness and a sub-gradient y

$$y = -\frac{\partial \psi}{\partial d(\phi)} = \mu\xi(\varepsilon - \frac{1}{2}\xi) \tag{4.2}$$

Applying (4.1) in 1D, we can get

$$g = \int_0^{l_c} y d'(\phi) d\phi \tag{4.3}$$

After calculation of the configurational force, we can get the normal velocity V by (2.21).

4.1.2 Comparison with the method in [1]

In [1], it applies the following formulation for the calculation of configurational force

$$g = \mu\xi(\varepsilon - 0.5\xi) \tag{4.4}$$

At the interface Γ_t, it applies the local driving force g, a function 4.4 of strain ε. As the strain ε is not constant during the diffuse interface, the driving force g is not

constant. Therefore, within the kinetic relation $V = Mg$, the interface velocity V varies during the diffuse interface. This will lead to varied thickness of the interface when updating the level set function ϕ. To keep the identical thickness, reinitializing ϕ is needed at every time step and the details please refer to [1]. This reinitializing treatment increase the computation cost.

However, the TLS method does not require this reinitializition in [1]. It takes advantage of the average driving force in the diffuse interface and moving the interface at the same speed caused by the average driving force.

4.2 FiGALE Method

4.2.1 Preliminaries

As the material velocity v and material acceleration a suffer jump discontinuities across certain interfaces $\Gamma_t \subset \Omega$, a new method 'FiGALE' is proposed applying the direction derivatives and fixed meshes. We define

$$\tilde{v} = D_V u \tag{4.5}$$

$$\tilde{a} = D_V \tilde{v} \tag{4.6}$$

where V is the interface velocity defined in (2.13), u is the material displacement. Hence, our new defined $\tilde{v}$, $\tilde{a}$ can overcome the jump discontinuities. Before applying the tilde quantities in the momentum equation, the relation between $\tilde{a}$ and material acceleration a is needed.

$$\tilde{v} = D_V u = v + u_{,X} V \tag{4.7}$$

$$\begin{aligned}
\tilde{a} = D_V \tilde{v} &= (v + u_{,X} V)_{,t} + (v + u_{,X} V)_{,X} V \\
&= a + (u_{,X} V)_{,t} + \tilde{v}_{,X} V \\
&= a + v_{,X} V + u_{,X} V_{,t} + \tilde{v}_{,X} V \\
&= a + 2\tilde{v}_{,X} V - (u_{,X} V)_{,X} V + u_{,X} V_{,t} \\
&= a + 2\tilde{v}_{,X} V - (u_{,X} V^2)_{,X} + u_{,X}(V_{,t} + V_{,X} V) \\
&= a + 2\tilde{v}_{,X} V - (u_{,X} V^2)_{,X} + u_{,X} D_V V
\end{aligned} \tag{4.8}$$

4.2.2 Formulations

Introducing (4.8) into the weakform (3.47) in 1D and applying the boundary conditions (2.23) results in

$$\begin{aligned}
\int_\Omega u^* \rho \tilde{a} d\Omega &= -\int_\Omega u^*_X \sigma d\Omega + \int_\Omega \rho \left[-2 \left(u^* V \right)_{,X} \tilde{v} + u^*_{,X} u_{,X} V^2 + u^* u_{,X} D_V V \right] \\
&= \int_\Omega u^*_X (-\sigma - 2\rho V \tilde{v} + \rho V^2 u_{,X}) d\Omega - \int_\Omega u^* \rho (2 V_{,X} \tilde{v} - (D_V V) u_{,X}) d\Omega
\end{aligned} \tag{4.9}$$

Considering the convection form in (4.9), we adopt SUPG to solve this problem. Take the same test function (3.62) in 1D and take $\alpha = 1$, we get $u^* = N + \frac{h}{2}N_{,X}$. Then (4.9) becomes

$$\begin{aligned}
&\int_\Omega (N + \frac{h}{2}N_{,X})\rho\tilde{a}d\Omega \\
&= \int_\Omega (N + \frac{h}{2}N_{,X})_{,X}(-\sigma - 2\rho V\tilde{v} + \rho V^2 u_{,X})d\Omega \\
&\quad - \int_\Omega (N + \frac{h}{2}N_{,X})\rho(2V_{,X}\tilde{v} - (D_V V)u_{,X})d\Omega \\
&= \int_\Omega N_{,X}(-\sigma - 2\rho V\tilde{v} + \rho V^2 u_{,X})d\Omega + \int_\Omega \frac{h}{2}N_{,XX}(-\sigma - 2\rho V\tilde{v} + \rho V^2 u_{,X})d\Omega \\
&\quad - \int_\Omega (N + \frac{h}{2}N_{,X})\rho(2V_{,X}\tilde{v} - (D_V V)u_{,X})d\Omega
\end{aligned} \tag{4.10}$$

Define the second part in right of (4.10) as II

$$\begin{aligned}
II &= \int_\Omega \frac{h}{2}N_{,XX}(-\sigma - 2\rho V\tilde{v} + \rho V^2 u_{,X})d\Omega \\
&= \int_\Gamma \frac{h}{2}N_{,X}(-\sigma - 2\rho V\tilde{v} + \rho V^2 u_{,X})d\Gamma - \int_\Omega \frac{h}{2}N_{,X}(-\sigma - 2\rho V\tilde{v} + \rho V^2 u_{,X})_{,X}d\Omega
\end{aligned} \tag{4.11}$$

Apply the boundary conditions, we can get

$$\int_\Gamma \frac{h}{2}N_{,X}(-\sigma - 2\rho V\tilde{v} + \rho V^2 u_{,X})d\Gamma = 0 \tag{4.12}$$

then

$$II = -\int_\Omega \frac{h}{2}N_{,X}(-\sigma_{,X} - 2\rho(V\tilde{v})_{,X} + \rho(V^2 u_{,X})_{,X})d\Omega \tag{4.13}$$

Introducing (4.13) into (4.10) and rearranging, we get

$$\begin{aligned}
&\int_\Omega (N + \frac{h}{2}N_{,X})\rho\tilde{a}d\Omega \\
&= -\int_\Omega N_{,X}\sigma d\Omega + \int_\Omega \frac{h}{2}N_{,X}\sigma_{,X}d\Omega + \int_\Omega h\rho N_{,X}V\tilde{v}_{,X}d\Omega \\
&\quad - \int_\Omega \frac{h}{2}\rho N_{,X}V^2 u_{,XX}d\Omega - \int_\Omega \left[2\rho V N_{,X} + 2\rho V_{,X}N\right]\tilde{v}d\Omega \\
&\quad + \int_\Omega \left[\rho V^2 N_{,X} - h\rho N_{,X}VV_{,X} + \rho(N + \frac{h}{2}N_{,X})D_V V\right]u_{,X}d\Omega
\end{aligned} \tag{4.14}$$

We define the finite element approximation of the motion $\mathbf{x}$, material displacement $\mathbf{u}$, direction velocity $\tilde{v}$, direction acceleration $\tilde{a}$

$$\mathbf{x}(\boldsymbol{\xi}^e) = \mathbf{x}_I N_I(\boldsymbol{\xi}^e) \tag{4.15}$$

$$\mathbf{u}(\boldsymbol{\xi}^e, t) = \mathbf{u}_I(t)N_I(\boldsymbol{\xi}^e) \tag{4.16}$$

$$\tilde{\mathbf{v}}(\boldsymbol{\xi}^e, t) = \tilde{\mathbf{v}}_I(t) N_I(\boldsymbol{\xi}^e) \tag{4.17}$$

$$\tilde{\mathbf{a}}(\boldsymbol{\xi}^e, t) = \tilde{\mathbf{a}}_I(t) N_I(\boldsymbol{\xi}^e) \tag{4.18}$$

Introduce (4.15)-(4.18) into (4.9). We get the matrices formulations

$$(M + M^s)\,\tilde{a} = -f^{int} + f^s - L^s\tilde{v} + Qu \tag{4.19}$$

where

$$\begin{aligned}
&M = I[M_{IJ}] = \int_\Omega \rho N_I N_J d\Omega; \quad M^s = I[M^s_{IJ}] = \int_\Omega \rho \frac{h}{2} N_{I,X} N_J d\Omega \\
&f^{int} = [f^{int}_I] = \int_\Omega N_{I,X}\sigma d\Omega; \quad f^s = [f^s_I] = \int_\Omega \frac{h}{2} N_{I,X}\sigma_{,X} d\Omega - \int_\Omega \rho \frac{h}{2} N_{I,X} u_{,XX} d\Omega \\
&L^s = I[L^s_{IJ}] = \int_\Omega \left[2\rho V N_{I,X} N_J + 2\rho V_{,X} N_I N_J + \rho h V N_{I,X} N_{J,X}\right] d\Omega \\
&Q = I[Q_{IJ}] = \int_\Omega \left[\rho V^2 N_{I,X} N_{J,X} - \rho h V V_{,X} N_{I,X} N_J + \rho D_V V (N_I N_{J,X} + \frac{h}{2} N_{I,X} N_{J,X})\right] d\Omega
\end{aligned} \tag{4.20}$$

Then we get the matrix formulations for FiGALE method.

4.2.3 Central difference time integral

In FiGALE, we apply the direction time derivatives of displacement. Therefore, we should also derive the relation between the material displacement $\mathbf{u}$, direction velocity $\tilde{v}$, and direction acceleration $\tilde{a}$ using central difference time integral method. The classical formulation of the central difference time integral

$$v^{n+1,p} = v^n + \frac{\triangle t}{2} a^n \tag{4.21}$$

$$u^{n+1,p} = u^n + \triangle t v^n + \frac{(\triangle t)^2}{2} a^n \tag{4.22}$$

$$v^{n+1} = v^{n+1,p} + \frac{\triangle t}{2} a^{n+1} \tag{4.23}$$

$$u^{n+1} = u^{n+1,p} \tag{4.24}$$

Replacing the material velocity v and material acceleration a by the directional velocity $\tilde{v}$ and directional acceleration $\tilde{a}$, respectively, we get the central difference formulation for FiGALE method.

$$\tilde{v}^{n+1,p}(x) = \tilde{v}^{n,p}(x - Vt) + \triangle t \tilde{a}^n(x - Vt) \tag{4.25}$$

$$u^{n+1,p}(x) = u^n(x - Vt) + \triangle t \tilde{v}^{n+1,p} \tag{4.26}$$

$$\tilde{v}^{n+1} = \tilde{v}^{n+1,p} + \frac{\triangle t}{2} \tilde{a}^{n+1} \tag{4.27}$$

$$u^{n+1} = u^{n+1,p} \tag{4.28}$$

4.2.4 Flowchart of FiGALE method

1. Update time:
   $t^{n+1} = t^n + \triangle t$

2. Compute the driving force at last time step t^n:
   Sharp interface theory:
   $g^n = \frac{1}{2}\mu\xi(\varepsilon^+ + \varepsilon^- - \xi)$
   Diffuse interface theory:
   $g^n = \int_0^{l_c} y d'(\phi) d\phi$

3. Compute interface velocity at last time step t^n:
   $w^n = Mg^n$

4. Update interface position:
   $\Gamma^{n+1} = \Gamma^n + w^n \triangle t$

5. Update predict displacement $\mathbf{u}^{n+1,p}$ and predict velocity $\mathbf{v}^{n+1,p}$
   $\tilde{v}^{n+1,p}(x) = \tilde{v}^{n,p}(x - Vt) + \triangle t \tilde{a}^n(x - Vt)$
   $u^{n+1,p}(x) = u^n(x - Vt) + \triangle t \tilde{v}^{n+1,p}$

6. Compute predict strain $\boldsymbol{\varepsilon}^{n+1,p} = \nabla \mathbf{u}^{n+1,p}$ and predict stress $\boldsymbol{\sigma}^{n+1,p}$
   $\boldsymbol{\sigma}^{n+1,p} = f(\boldsymbol{\varepsilon}^{n+1,p})$

7. Solve matrix equation to get acceleration $\mathbf{a}^{n+1}$
   $(M + M^s)\,\tilde{a} = -f^{int} + f^s - L^s\tilde{v} + Qu$

8. Update displacement $\mathbf{u}^{n+1}$ and velocity $\mathbf{v}^{n+1}$
   $\tilde{v}^{n+1} = \tilde{v}^{n+1,p} + \frac{\triangle t}{2}\tilde{a}^{n+1}$
   $u^{n+1} = u^{n+1,p}$

9. Update strain $\boldsymbol{\varepsilon}^{n+1} = \nabla \mathbf{u}^{n+1}$ and stress $\boldsymbol{\sigma}^{n+1}$
   $\boldsymbol{\varepsilon}^{n+1} = \nabla \mathbf{u}^{n+1}$
   $\boldsymbol{\sigma}^{n+1} = f(\boldsymbol{\varepsilon}^{n+1})$

Chapter 5

Numerical Results

In this chapter, several representative numerical simulations are shown to illustrate the dynamic performance of the rubber band with phase changing using two theories (sharp interface theory and diffuse interface theory) and three numerical methods (Lagrangian method, ALE method and FiGALE methods). We consider the dynamic evolution of a twin nucleus in a one-dimensional domain $\Omega = [0, 1]$, subject to displacement boundary conditions corresponding to constant applied small shear loading, shown in Fig. 5. We apply the Dirichlet boundary condition $u = ky$ on $\partial\Omega$. Both quasi-static and dynamic conditions are considered in these model examples. Considering the round-off errors in time integration, the time step is chosen as $\triangle t = 0.9\triangle t_{cr}$, where $\triangle t_{cr} = h/c$. Non-dimensionalizing is also used. Other parameters are set: strain vector $\xi = 0.01$, $k = 0.011$,$M = 0.01$.

The first example is our referential numerical solution using a fine Lagrangian mesh and the diffuse interface theory. The three numerical methods are compared using sharp interface theory in Example 2 and diffuse interface theory in Example 3.

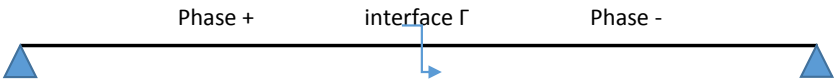

Figure 5.1: Phase changing

5.1 Example 1: Referential numerical solution

Our referential numerical solution is got through using both the diffuse interface theory and Lagrangian mesh while applying fine mesh $h = 0.001$.

The initial displacement and initial strain are shown in Fig. 5.2 and Fig 5.3, respectively. We can see that the displacement is continuous while the singularity of the strain is smoothing treated by a level set method. As the dynamic happens, the total energy in Fig 5.4 decrease in time, which is expected.

The interface tip in Fig 5.5 is moving towards to the low strain phase, which means the low strain phase turns into high strain phase. We have to notice that the high strain phase is also in the low energy well while the low strain phase is in the high energy well. Then the phenomena shows that the low energy phase is swallowing the high energy phase, that is, the low energy phase is more stable.

The interface velocity in Fig 5.7 decrease in time and we can expect that if the rubber band is long enough, the interface will finally go to zero and we can get a stable dynamics in the rubber band. The tendency of driving force g in Fig 5.6 and interface velocity w are the same, which is in agreement with the linear kinetic relation in Eq.2.21.

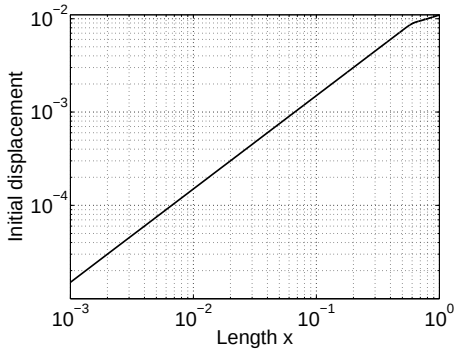

Figure 5.2: Initial displacement

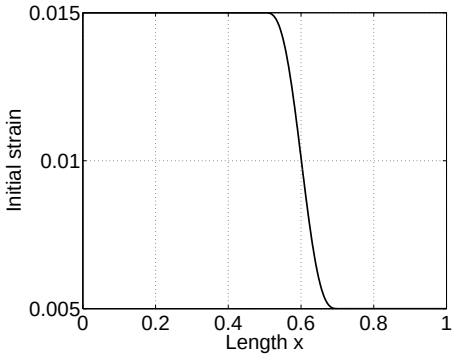

Figure 5.3: Initial strain

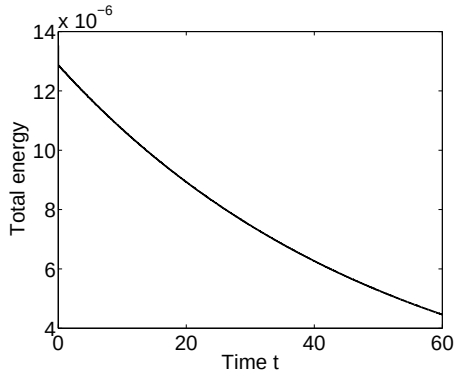

Figure 5.4: Total energy in time

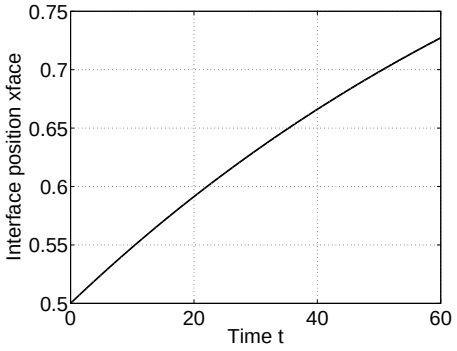

Figure 5.5: Interface tip position in time

5.2 Example 2: Comparison of methods in sharp interface theory

We analyze the methods in sharp interface theory. Simulations are done using Lagrangian, ALE and FiGALE methods. The mesh size is $h = 0.01$. In sharp interface, the thickness of the interface is regarded as zero and singularity of the strain is a direct jump across the interface. Because there is discontinuous in strain using sharp interface, we know that the results must be unstable or oscillation will happen very soon. Then, we just apply a considerately short time $t = 10$.

Results in Fig 5.8 show that the stress will oscillate using Lagrangian and FiGALE methods and ALE method.

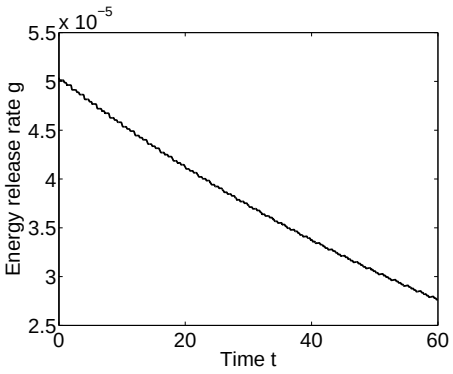

Figure 5.6: Driving force g in time

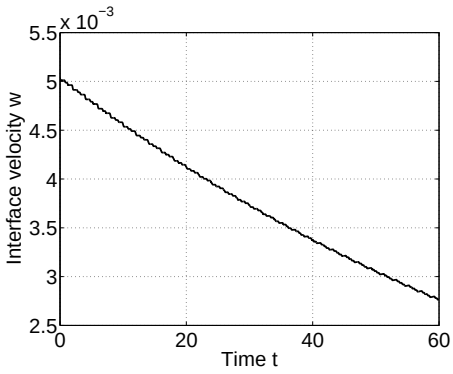

Figure 5.7: Interface velocity in time

In Fig 5.8a,5.8c and 5.8e, we can see that the displacements using ALE methods are stable in the beginning $t < 2$. When the time $t > 5$, the magnitude of the displacement using ALE methods is the biggest while the magnitude of the displacement using FiGALE is the smallest. The results using Lagrangian method and FiGALE method are more close, while a bit far away from the ALE methods

Fig 5.8b,5.8d and 5.8f, the magnitude of the tress using ALE methods is the smaller than that using Lagrangian method while the magnitude of the stress using FiGALE is the smallest.

In Fig 5.8h, the interface using ALE methods goes faster than that using Lagrangian method and FiGALE method.

Therefore, in sharp interface theory, FiGALE method is the best among the three methods.

5.3 Example 3: Comparison of methods in diffuse interface theory

In this section, We analyze the methods in diffuse interface theory. Simulations are done using Lagrangian method, ALE methods and FiGALE method. Here, we apply the coarse mesh size $h = 0.01$. We compare the displacement and stress evolution in time.

We highlight the stress at time $t = 10, 40$. Fig.5.3 shows that there is not much difference in stress between Lagrangian and ALE methods, while the stress using FiGALE method looks more smoothing.

In order to get more clear results, we take into account the displacement and stress evolution at three different points with initial position $X = 0.3, 0.5, 0.7$ and compare the results with the referential simulation results in Example 1. The displacement and stress evolution at point $X = 0.5$ are highlighted in Fig 5.3e and Fig 5.3f.

Results in Fig. 5.3 shows that at the beginning, the results (displacement or stress) are very close. However, when the time become considerably long, the results

using Lagrangian method and ALE methods begin to separate, and the ALE results decrease slower than the Lagrangian results. Although the FiGALE results contain small oscillation, its tendency are more close to the referential results.

5.4 Conclusion

Simulations are investigated using three numerical methods, Lagrangian method, ALE methods and FiGALE method, as well as two interface theory, sharp interface theory and diffuse interface theory. Results in Fig 5.8 using the sharp interface theory oscillate and show that FiGALE is the best among the three methods. The oscillation is because there are discontinuity in the velocity, which can be derived from the jump conditions and discontinuous initial strain.

More attentions are paid to the diffuse interface theory. First, we apply the fine mesh $h = 0.001$ and Lagrangian method as our referential results. In this referential simulation, we observe the evolution of total energy, interface, driving force and the interface velocity, which give us general understanding of the dynamics of the rubber band with phase changing. Afterwards, simulations are conducted using Lagrange method, ALE methods and FiGALE method with the same coarse mesh size $h = 0.01$. Results show that in short time steps, the Lagrangian and ALE results are quite similar; in long time steps FiGALE results are more close to the referential results while FiGALE results contain small oscillations, and ALE results are a bit more close to referential results compared to the Lagrangian results. ALE results do not contain oscillation and in this aspect it is better than FiGALE method. This conclusion can be shown more clear in Tab. 5.1.

Future research should extend to more complicate situations, such as plasticity constitution problem instead of elasticity, implicit time integration schemes instead of explicit time integration schemes. Both plasticity and implicit time integration will lead to non-linear computation, therefore, Newton Raphson is involved. Higher dimensions can be investigate to check this new proposed method FiGALE.

	Lagrangian	ALE	FiGALE
Sharp interface	$--$	$--$	$-$
Diffuse interface	$++$	$+++$	$+++$

Notes: $--$ stands for worse, $-$ stands for bad; $++$ stands for good, $+++$ stands for better.

Table 5.1: Conclusion of Lagrangian, ALE and FiGALE methods

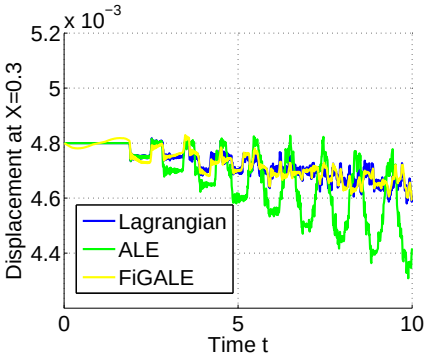

(a) Displacement evolution at $X = 0.3$

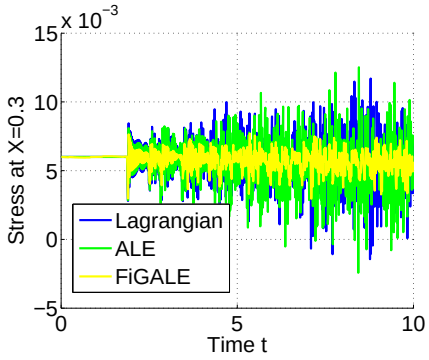

(b) Stress evolution at $X = 0.3$

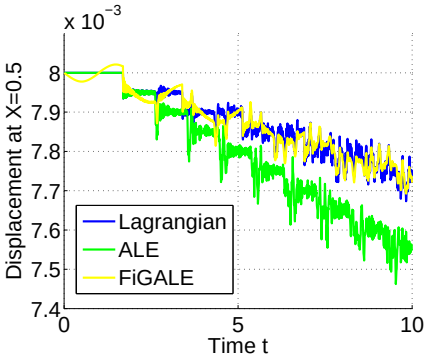

(c) Displacement evolution at $X = 0.5$

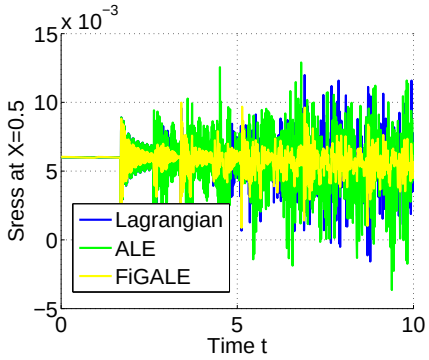

(d) Stress evolution at $X = 0.5$

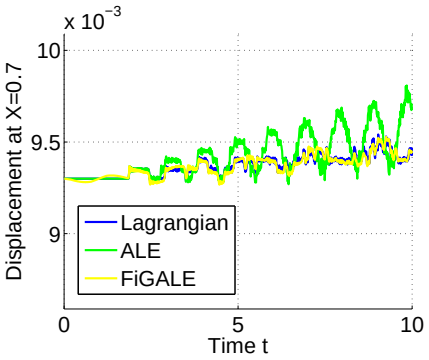

(e) Displacement evolution at $X = 0.7$

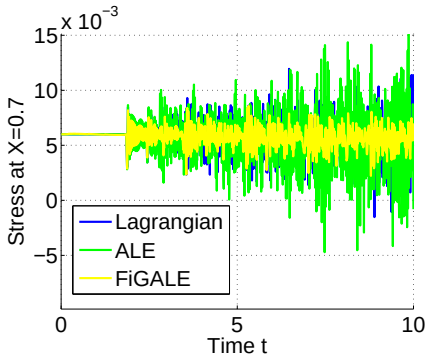

(f) Stress evolution at $X = 0.7$

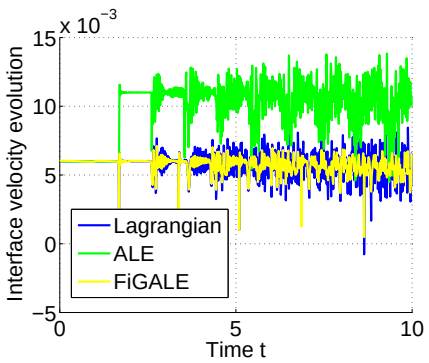

(g) Interface velocity evolution

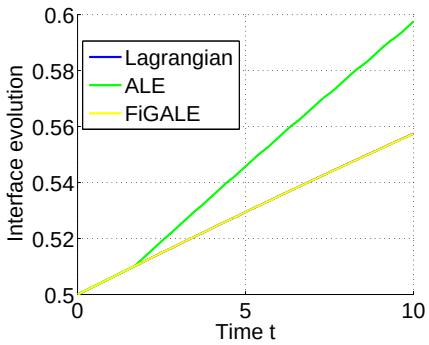

(h) Interface evolution

Figure 5.8: Lagrangian, ALE and FiGALE in sharp interface

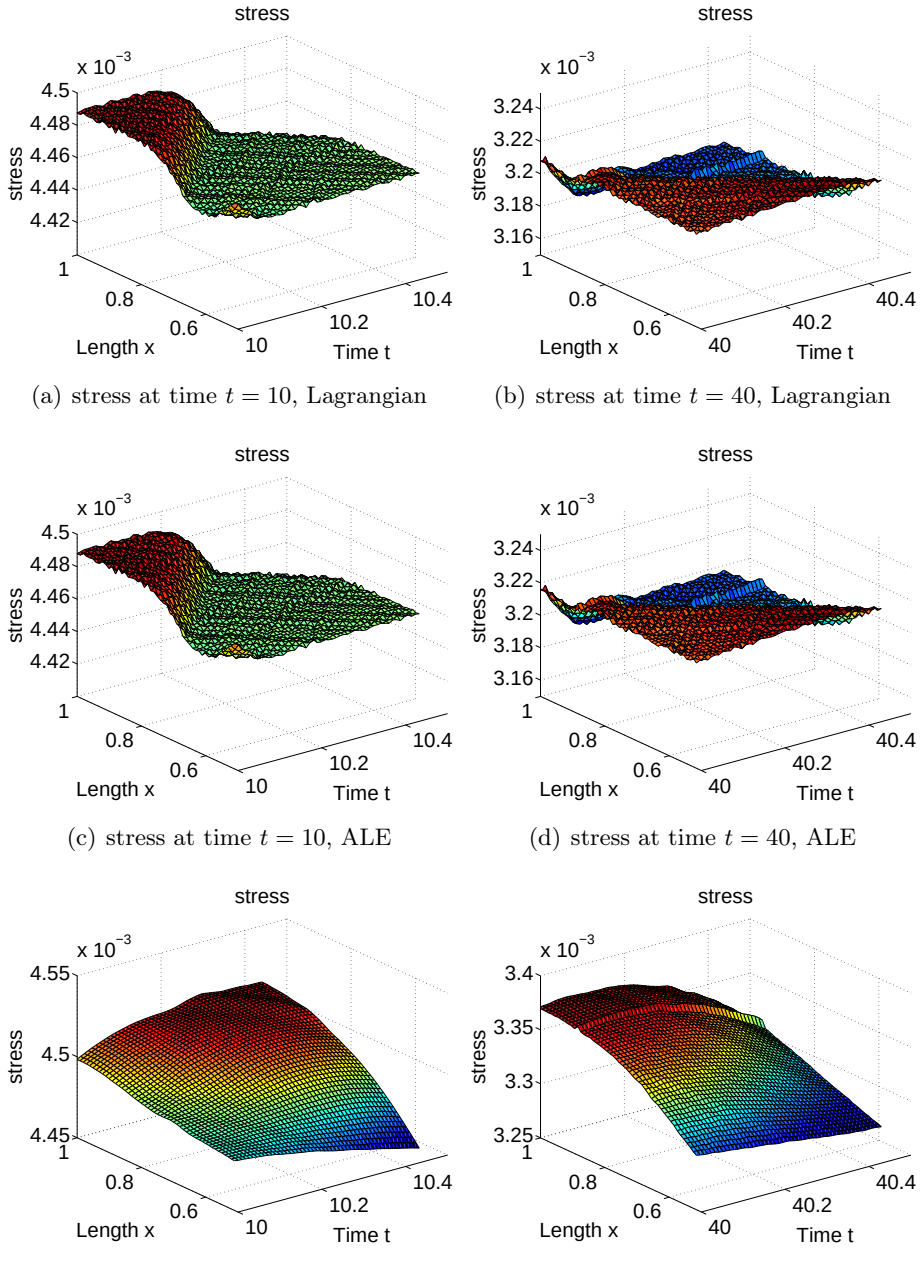

(a) stress at time $t = 10$, Lagrangian

(b) stress at time $t = 40$, Lagrangian

(c) stress at time $t = 10$, ALE

(d) stress at time $t = 40$, ALE

(e) stress at time $t = 10$, FiGALE

(f) stress at time $t = 40$, FiGALE

Figure 5.9: Comparison of stress using Lagrangian, ALE and FiGALE methods in diffuse interface theory at time $t = 10, 20, 40$

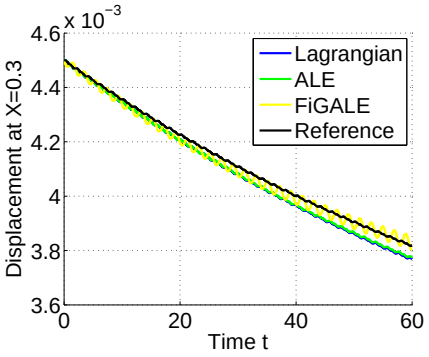

(a) Displacement evolution at $X = 0.3$

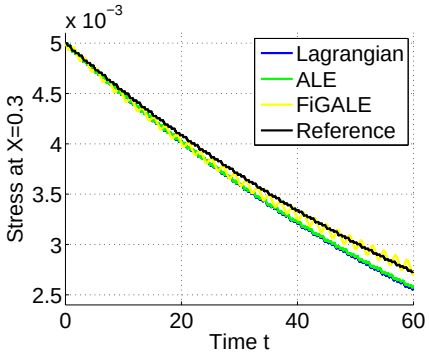

(b) Stress evolution at $X = 0.3$

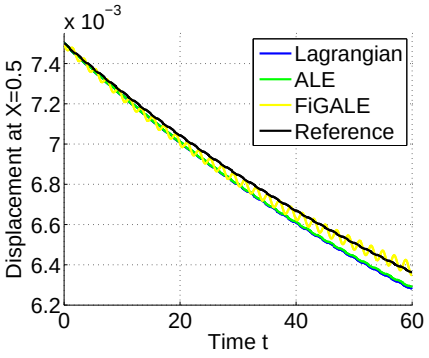

(c) Displacement evolution at $X = 0.5$

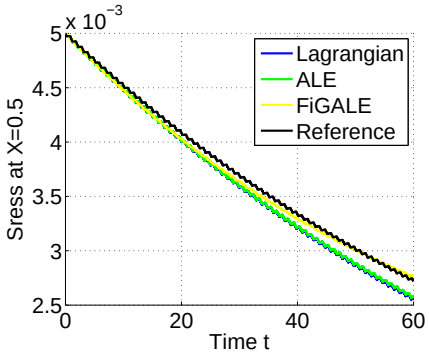

(d) Stress evolution at $X = 0.5$

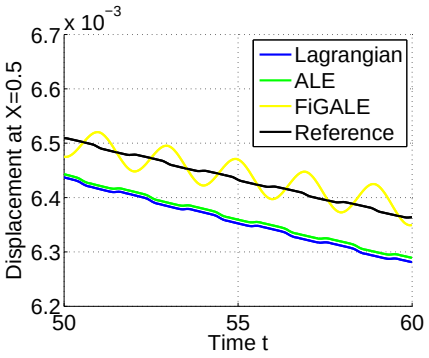

(e) Highlight Displacement at $X = 0.5$

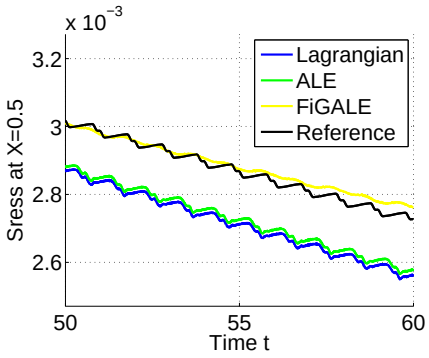

(f) Highlight Stress at $X = 0.5$

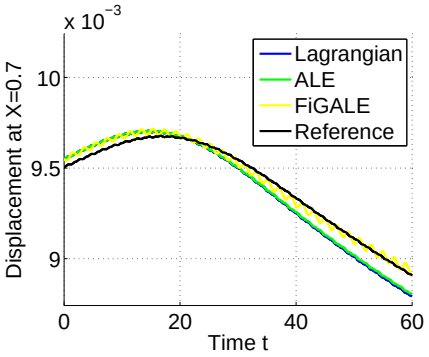

(g) Displacement evolution at $X = 0.7$

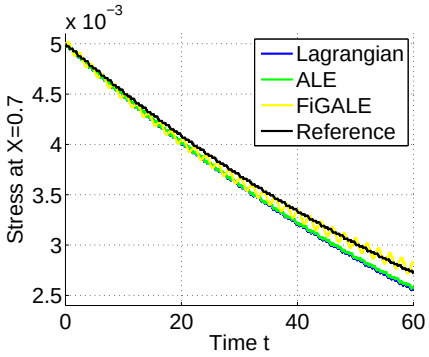

(h) Stress evolution at $X = 0.7$

Figure 5.10: Displacement and stress evolution at points $X = 0.3, 0.5, 0.7$ using Lagrangian, ALE and FiGALE methods in diffuse interface theory

Bibliography

[1] Hou Thomas Y, Rosakis Phoebus, LeFloch Philippe, "A level-set approach to the computation of twinning and phase-transition dynamics," *Journal of Computational Physics*, vol. 150, pp. 302–331, Apr. 1999. (Cited on pages 5, 13, 33 and 34.)

[2] Christian JW, Mahajan S, "Deformation twinning," *Progress in materials science*, vol. 39, pp. 1–157, 1995. (Cited on page 10.)

[3] Rosakis P, Tsai H, "Dynamic twinning processes in crystals," *International journal of solids and structures*, vol. 32, pp. 2711–2723, 1995. (Cited on pages 10, 11, 12, 13 and 14.)

[4] William C Johnson, "Precipitate shape evolution under applied stress thermodynamics and kinetics," *Metallurgical and Materials Transactions A*, vol. 18, no. 2, pp. 233–247, 1987. (Cited on page 10.)

[5] Johnson WC, Voorhees PW, Zupon DF, "The effect of elastic pressure on the kinetics oswald ripening: Two particle problem," *Metallurgical and Materials Transactions A*, vol. 20A, no. 7, p. 1175, 1989. (Cited on page 10.)

[6] Johnson WC, Abinandanan TA, Voorhees PW, "The coarsening kinetics of two misfitting particles in an anisotropic crystal," *Acta Materialia*, vol. 38, pp. 1349–1367, 1990. (Cited on page 10.)

[7] Jou HJ, Leo PH, Lowengrub JS, "Microstructural evolution in inhomogeneous elastic media," *Computational Physics*, vol. 131, no. 1, pp. 109–148, 1997. (Cited on page 10.)

[8] Socrate S, Parks DM, "Numerical determination of the elastic driving force for directional coarsening in ni-superalloys," *Acta Metallurgica et Materialia*, vol. 41, p. 2185, 1993. (Cited on page 10.)

[9] Thompson ME, Su CS, Voorhees PW, "The equilibrium shape of a misfitting precipitate," *Acta Metallurgica et Materialia*, vol. 42, no. 6, pp. 2107–2122, 1994. (Cited on page 10.)

[10] Su CH, Voorhees PW, "The dynamics of precipitate evolution in elastically stressed solids-i. inverse coarsening," *Acta Materialia*, vol. 44, no. 5, pp. 1987–1999, 1996. (Cited on page 10.)

[11] Su CH, Voorhees PW, "The dynamics of precipitate evolution in elastically stressed solids-ii. particle alignment," *Acta Materialia*, vol. 44, no. 5, pp. 2001–2016, 1996. (Cited on page 10.)

[12] Voorhees PW, McFadden GB, Boisvert RF, Meiron DI, "Numerical simulation of morphological development during ostwald ripening," *Acta Metall*, vol. 36, p. 207, 1988. (Cited on page 10.)

[13] Voorhees PW, McFadden GB, Johnson WC, "On the morphological development of second-phase particles in elastically stressed solids," *Acta Metall.*, vol. 40, p. 2979, 1992. (Cited on page 10.)

[14] Rosakis P, Tsai H, Rosakis P, Tsai HY, "On the role of shear instability in the modeling of crystal twinning," *Mechanics of Materials*, vol. 12, p. 245, Mar. 1994. (Cited on pages 11 and 12.)

[15] Rosakis P, "Compact zones of shear transformation in an anisotropic solid," *Journal of the Mechanics and Physics of Solids*, vol. 40, no. 6, pp. 1163–1195, 1992. (Cited on page 11.)

[16] Bunshah RF, "Rates of deformation twinning in metals," in *Deformation Twinning*, pp. 390–392, 1964. (Cited on page 11.)

[17] Tsai H, Rosakis P, "On anisotropic compressible materials that can sustain elastodynamic anti- plane shear," *Elasticity*, vol. 35, pp. 213–222, 1994. (Cited on page 11.)

[18] Osher Stanley, Sethian A James, "Fronts propagating with curvaturedependent speed: algorithms based on hamilton-jacobi formulations," *Journal of Computational Physics*, vol. 79, no. 1, pp. 12–49, 1988. (Cited on page 11.)

[19] Abeyaratne R, Knowles JK, "On the driving traction acting on a surface of strain discontinuity in a continuum," *Journal of the Mechanics and Physics of Solids*, vol. 38, pp. 345–360, Jan. 1990. (Cited on pages 12 and 13.)

[20] Abeyaratne R, Knowles JK, "Kinetic relations and the propagation of phase boundaries in solids," *Archive for rational mechanics and analysis*, vol. 114, pp. 119–154, 1991. (Cited on page 13.)

[21] Khachaturyan AG, Semenovskaya SV, Morris JW, "Theoretical analysis of strain induced shape cchange in cubic pprecipitate during coarsening," *Acta metall*, vol. 36, pp. 1563–1572, 1988. (Cited on page 14.)

[22] McCormack M, Khatchaturyan AG,Jr Morris JW, "A two dimensional analysis of the evolution of coherent precipitate in elastic media," *Acta metall*, vol. 40, p. 325, 1992. (Cited on page 14.)

[23] Wang Y, Chen LQ, Khachaturyan AG, "Kinetics of the strain-induced morphological transformation in cubic alloys with miscibility gap," *Acta Metall*, vol. 41, p. 279, 1993. (Cited on page 14.)

[24] Wang Yunzhi, Khachaturyan AG, "Shape instability during precipitate growth in coherent solids," *Acta metall*, vol. 43, p. 1837, 1995. (Cited on page 14.)

[25] Lee JK, "Coherency strain analyses via a discrete atom method," *Scripta Metallurgica et Materialia*, vol. 32, no. 4, pp. 559–564, 1995. (Cited on page 14.)

[26] Yue Pengtao, Zhou Chunfeng, Feng James J, "Spontaneous shrinkage of drops and mass conservation in phase-field simulations," *Journal of Computational Physics*, vol. 223, pp. 1–9, Apr. 2007. (Cited on page 14.)

[27] Sussman Mark, Almgren Ann S, Bell John B, Colella Phillip, Howell Louis H, Welcome Michael L, "An adaptive level set approach for incompressible two-phase flows," *Journal of Computational Physics*, vol. 148, pp. 81–124, 1999. (Cited on page 14.)

[28] Stéphane Popinet, "An accurate adaptive solver for surface-tension-driven interfacial flows," *Journal of Computational Physics*, vol. 228, pp. 5838–5866, 2009. (Cited on page 14.)

[29] Ding Hang, Yuan Chengjun, "On the diffuse interface method using a dual-resolution cartesian grid," *Journal of Computational Physics*, vol. 273, pp. 243–254, Sept. 2014. (Cited on pages 14 and 15.)

[30] Brackbill JU, Kothe DB, Zemach C, "A continuum method for modeling surface tension," *Journal of Computational Physics*, vol. 100, pp. 335–354, 1992. (Cited on page 15.)

[31] Noh WF, "Cel: A time dependent, two space dimensional, coupled eulerian lagrange code," in *Methods in Computational Physics*, pp. 117–179, 1964. (Cited on page 16.)

[32] Trulio JG, *Theory and Structure of the AFTON Codes.* Defense Technical Information Center, 1966. (Cited on page 16.)

[33] Hirt CW, Amsden AA, Cook JL, "An arbitrary lagrangian-eulerian computing method for all flow speeds," *Journal of Computational Physics*, vol. 14, pp. 227–253, 1974. (Cited on page 16.)

[34] Hughes TJR, Liu WK, Zimmermann TK, "Lagrangian-eulerian finite element formulation for incompressible viscous flows," *Computer Methods in and Engineering*, vol. 29, no. 3, pp. 329–349, 1981. (Cited on page 16.)

[35] Belytschko T, Kennedy JM, "Computer models for subassembly simulation," *Nuclear Engineering and Design*, vol. 49, no. 1-2, pp. 17–38, 1978. (Cited on page 16.)

[36] Belytschko T, Kennedy JM, Schoeberle DF, "Quasi-eulerian finite element formulation for fluid-structure interaction," *J. Pressure Vessel Technol.*, vol. 102, no. 1, pp. 62–69, 1980. (Cited on page 16.)

[37] Donea J, Giuliani S, Halleux JP, "An arbitrary lagrangian-eulerian finite element method for transient dynamic fluid-structure interactions," *Computer Methods in Applied Mechanics and Engineering*, vol. 33, no. 1-3, pp. 689–723, 1982. (Cited on page 16.)

[38] Belytschko T, "Fluid-structure interaction," *Computers Structures*, vol. 12, pp. 459–469, Oct. 1980. (Cited on page 16.)

[39] Kennedy JM, Belytschko T, "Theory and application of a finite element method for arbitrary lagrangian-eulerian fluids and structures," *Nuclear engineering and design*, vol. 68, pp. 129–146, 1981. (Cited on page 16.)

[40] Liu WK, Belytschko T, Chang H, "An arbitrary lagrangian-eulerian finite element method for path-dependent materials," *Computer Methods in Applied Mechanics*, vol. 58, pp. 227–245, 1986. (Cited on pages 16 and 17.)

[41] Benson J David, "An efficient, accurate, simple ale method for nonlinear finite element programs," *Computer Methods in Applied Mechanics and Engineering*, vol. 72, pp. 305–350, Mar. 1989. (Cited on page 16.)

[42] Codina Ramon, Houzeaux Guillaume, Owen Herbert Coppola, Baiges Joan, "The fixed-mesh ale approach for the numerical approximation of flows in moving domains," *Journal of Computational Physics*, vol. 228, no. 5, pp. 1591–1611, 2009. (Cited on page 16.)

[43] Sawada Tomohiro, Hisada Toshiaki, "Fluid-structure interaction analysis of the two-dimensional flag-in-wind problem by an interface-tracking ale finite element method," *Computers Fluids*, vol. 36, pp. 136–146, Jan. 2007. (Cited on page 16.)

[44] Zhang J, Childress S, Libchaber A, Shelley M, "Flexible filaments in a flowing soap film as a model for one-dimensional flags in a two-dimensional wind," *Nature*, vol. 408, pp. 835–9, Dec. 2000. (Cited on page 16.)

[45] Brooks N Alexander, Hughes TJR, "Streamline upwind petrov-galerkin formulations for convection dominated flows with particular emphasis on the incompressible navier-stokes equations," *Computer Methods in Applied Mechanics and Engineering*, vol. 32, pp. 199–259, 1982. (Cited on page 17.)

[46] Liu WK, Chang Herman, Chen Jiun-Shyan, Belytschko T, "Arbitrary lagrangian-eulerian petrov-galerkin finite elements for nonlinear continua," *Computer methods in applied Mechanics*, vol. 68, pp. 259–310, 1988. (Cited on page 17.)

[47] Zienkiewicz OC, Taylor RL, Nithiarasu P, *The Finite Element Method for Fluid Dynamics*. 2014. (Cited on page 17.)

[48] Belytschko T, Kennedy JM, "Computer modells for subassembly simulation," *Nuclear Engineering and Design*, vol. 49, pp. 17–38, 1978. (Cited on page 17.)

[49] Liu WK, "Finite element procedures for fluid-structure interaction and application to liquid storage tanks," *Nuclear Engineering and Design*, vol. 65, pp. 221–238, 1981. (Cited on page 17.)

[50] Hughes TJR, Liu WK, Zimmermann TK, "Lagrangian-eulerian finite element formulation for incompressible viscous fows," *Computer Methods in Applied Mechanics and Engineering*, vol. 29, pp. 329–349, 1981. (Cited on page 17.)

[51] Huerta A, Liu WK, "Viscous flow with large free surface motion," *Computer Methods in Applied Mechanics and Engineering*, vol. 69, pp. 277–324, 1988. (Cited on page 17.)

[52] Nomura T, Hughes TJR, "An arbitrary lagrangian eulerian finite element method for interaction of fluid and a rigid body," *Computer Methods in Applied Mechanics and Engineering*, vol. 95, pp. 115–138, 1992. (Cited on page 17.)

[53] Yamada T, Kikuchi F, "An arbitrary lagrangian eulerian finite element method for incompressible hyperelasticity," *Computer Methods in Applied Mechanics and Engineering*, vol. 102, pp. 149–177, 1993. (Cited on page 17.)

[54] Wall WA, Ramm E, "A stabilized finite element method for incompressiblenavier-stokes on time dependent domains," in *the Fourth U.S. National Congress on Computational Mechanics*, (San Francisco), 1997. (Cited on page 17.)

[55] Wall WA, Ramm E, "Fluid-structure interaction based upon a stabilized ale finite element method," in *Computational Mechanics New Trends and Applications*, (Barcelona, Spain), CIMNE, 1998. (Cited on page 17.)

[56] Armero Francisco, Love Edward, "An arbitrary lagrangian eulerian finte element method for finite strain plasticity," *International Journal for Numerical Methods in Engineering*, vol. 57, pp. 471–508, 2003. (Cited on page 17.)

[57] Dokainish MA, Subbaraj K, "A survey of direct time-integration methods in computational structural dynamics-i. explicit methods," *Computers & Structures*, vol. 32, no. 6, pp. 1371–1386, 1989. (Cited on page 18.)

[58] Krieg RD, "Unconditional stability in numerical time integration methods," *Journal of Applied Mechanics*, vol. 40, no. 2, p. 417, 1973. (Cited on page 18.)

[59] Dahlquist G, Björck A, *Numerical Methods*. Courier Dover Publications, 2003. (Cited on page 18.)

[60] Braekhus J, Aasen JO, "Experiments with direct integration algorithms for ordinary differential equations in structural dynamics," *Computers Structures*, vol. 13, pp. 95–96, 1981. (Cited on page 18.)

[61] Jensen PS, "Transient analysis of structures by stiffly stable methods," *Computers Structures*, vol. 4, pp. 615–626, 1974. (Cited on page 18.)

[62] Park KC , Felippa CA, Deruntz JA, *Computational Methods for Fluid Structure-Interaction Problems*, vol. 26, ch. Stabilization of staggered solution procedures for fluid-structure interaction analysis, pp. 95–124. ASME Applied Mechanics Symposia, 1977. (Cited on page 18.)

[63] Marfurt Kurt J, "Accuracy of finite difference and finite element modeling of the scalar and elastic wave equations," *GEOPHYSICS*, vol. 49, pp. 533–549, May 1984. (Cited on page 18.)

[64] Fujii H, Oden JT, Clough RW, Yamamoto Y, *Advances in Computational Methods in Structural Mechanics and Design*, ch. Finite element schemes: stability and convergence, pp. 201–218. UAH Press, 1972. (Cited on page 18.)

[65] Krieg RD, Key SW, "Transient shell response by numerical time integration," *International Journal for Numerical Methods in Engineering*, vol. 17, pp. 273–286, 1973. (Cited on page 18.)

[66] Leech JW, Hsu P, Mack EW, "Stability of a finite difference method for solving matrix equations," *AIAA Journal*, vol. 3, pp. 2172–2173, 1965. (Cited on page 18.)

[67] Hughes TJR, Liu WK, "Implicit-explicit finite elements in transient analysis: Stability theory," *Journal of Applied Mechanics*, vol. 45, pp. 371–374, 1978. (Cited on page 18.)

[68] Levy S, Kroll WD, "Errors introduced by finite space and time increments in dynamic response computations," in *First U.S. Nat. Conf. on Appl. Mech.*, pp. 1–8, 1951. (Cited on page 18.)

[69] Park KC, "Practical aspects of numerical time integration," *Computers Structures*, vol. 7, pp. 343–353, 1977. (Cited on page 18.)

[70] Oden JT, Frost RB, "Convergence, accuracy and stability of finite element approximations for a class of nonlinear hyperbolic equations," *International Journal for Numerical Methods in Engineering*, vol. 6, pp. 357–362, 1973. (Cited on page 18.)

[71] Mallen R, Belytschko T, "An analysis of an unconditionally stable explicit method," *Computers Structures*, vol. 16, pp. 691–699, 1983. (Cited on page 18.)

[72] Belytschko T, "A survey of numerical methods and computer programs for dynamic structural analysis," *Nuclear Engineering and Design*, vol. 37, no. 1, pp. 23–24, 1976. (Cited on page 18.)

[73] Belytschko T, Liu WK, Moran Brian, *Nonlinear Finite Elements For Continua And Structures*, vol. 104. 2000. (Cited on pages 19 and 30.)

[74] Moës N, Stolz C, Bernard PE, Chevaugeon N, "A level set based model for damage growth: the thick level set approach," *International Journal for Numerical Methods in Engineering*, no. December 2010, pp. 358–380, 2011. (Cited on page 33.)